SIAM J. NUMER. ANAL.
Vol. 50, No. 6, pp. 3375–3401

STABILITY ANALYSIS OF INTERFACE TEMPORAL DISCRETIZATION IN GRID OVERLAPPING METHODS*

YULIA T. PEET† AND PAUL F. FISCHER‡

Abstract. We investigate the stability of a temporal discretization of interface terms in grid overlapping methods. A matrix stability analysis is performed on a model problem of the one-dimensional diffusion equation on overlapping grids. The scheme stability is first analyzed theoretically, and a proof of the unconditional stability of the first-order interface extrapolation scheme with the first- and second-order time integration for any overlap size is presented. For the higher-order schemes, we obtain explicit estimates of the spectral radius of the corresponding discrete matrix operator and document the values of the stability threshold depending on the number of grid points and the size of overlap. The influence of iterations on stability properties is also investigated. Numerical experiments are then presented relating the obtained stability bounds to the observed numerical values. Semidiscrete analysis confirms the derived scaling for the stability bounds.

Key words. grid overlapping methods, temporal stability, explicit interface extrapolation, backward-differentiation scheme, matrix analysis

AMS subject classifications. 65M12, 65M55, 65F15

DOI. 10.1137/110831234

1. Introduction.

The idea of splitting a computational domain into smaller subdomains and reconstructing the global solution by coupling individual solutions has been around for several decades. The motivation for such decomposition can vary: to accelerate the solution of large linear systems (domain decomposition) [6], [26], [36], to alleviate grid construction in complex geometries (composite grid methods) [7], [24], [38], or to achieve the integrated solution of multiphysics problems (integrative simulations) [17], [29], [34]. The strategy of how this decomposition is performed can be further classified into nonoverlapping [2], [5], [8], [15], [22] and overlapping grid methods [7], [21], [29], [35], [42].

The current paper is motivated by our recent development of a composite grid method with overlapping subdomains for solving incompressible unsteady Navier–Stokes equations [30]. With overlapping grid methods, equations have to be coupled across the subdomains by the condition of matching variables at the subdomain interfaces. Interface variables are expressed through the interior variables of an adjacent subdomain with the help of an interpolation stencil. This matching can be enforced either implicitly or explicitly in time. With an implicit formulation, the coupling relations are to be solved implicitly by either iterative or direct methods [7], [41]. This method can be viewed as an analogue to substructuring methods for nonoverlapping domains [22], [28], [36]. With an explicit interface formulation, interface values are also expressed through interior values of an adjacent subdomain with the help of an

*Received by the editors April 18, 2011; accepted for publication (in revised form) October 2, 2012; published electronically December 19, 2012. We acknowledge the financial support of this work by NSF RTG grant DMS-0636574 and the SHARP project of the U.S. Department of Energy under contract DE-AC02-06CH11357.

http://www.siam.org/journals/sinum/50-6/83123.html

†Department of Engineering Sciences and Applied Mathematics, Northwestern University, Evanston, IL 60208, and Mathematics and Computer Science Division, Argonne National Laboratory, Argonne, IL 60439. Current affiliation: School for Engineering of Matter, Transport and Energy, Arizona State University, Tempe, AZ 85287 (ypeet@asu.edu).

‡Mathematics and Computer Science Division, Argonne National Laboratory, Argonne, IL 60439 (fischer@mcs.anl.gov).

interpolation stencil, but explicitly. Since the interface values are set explicitly, there is no guarantee that they will still match at the end of a time step unless some kind of iteration procedure is implemented. In order to eliminate a possible mismatch, the majority of explicit interface grid overlapping methods use a Schwarz-like iteration procedure [35] at each time step to guarantee the convergence of interface values (also called intergrid iteration or the iteration-by-subdomain approach) [16], [25], [37], [39], [43]. With the iteration-by-subdomain approach, equations are advanced by one iteration followed by interface conditions exchange, advanced by one iteration again, and so on until global convergence.

Achieving global convergence of the boundary value problem across the computational domain is an expensive process: thus, in incompressible flow simulations with fractional/splitting step methods, the solution of the elliptic Poisson equation for pressure takes up most of the computational time per time step. Introducing a global iterative loop for other variables (velocities, temperature, etc.) across overlapping subdomains can increase the computational time significantly. The convergence rate of Schwarz methods applied to singularly perturbed elliptic operators (arising in unsteady problems) has been found to deteriorate significantly when the overlap size decreases or the time step increases [4], [33]. Indeed, some schemes with intergrid iterations can take several hundreds of iterations to reach global convergence of the variables across subdomains [39]. Therefore, the question arises whether it is necessary to pay such a price for the perfect match of all the interface values. Motivation for driving interface values to convergence might be twofold: considerations of accuracy and stability. However, if the interface conditions are not strictly matching at the end of a time step but are merely consistent [43] (the difference is of the same spatial and temporal accuracy as that of the overall solution method), the overall accuracy of a noniterative scheme would not be lowered by the interface conditions mismatch. To achieve spatial consistency, attention must be paid to a choice of an interpolation stencil [3], [7]. For temporal consistency, we have proposed a novel idea of extrapolating interface values in time with the same (or higher) order of accuracy than that of the integration scheme.

As follows from the previous discussion, Schwarz iterations are unnecessary for consistent schemes from the viewpoint of accuracy. The stability question, however, remains. Although studies of convergence properties of iterative schemes, including Schwarz multiplicative and additive methods, are plentiful (see, for example, [21], [36], and references therein), investigations of stability of domain decomposition methods when iterations are eliminated or at least reduced are scarce. A majority of research on stability concerns nonoverlapping grids [1], [5], [31], [32]. Some limited stability studies in overlapping grid framework were performed by Gao and He [12] for parabolic problems and by Pärt-Evander and Sjögreen [27] for hyperbolic problems, in a situation of either fully implicit [12] or first-order explicit [27] coupling.

The goal of the current paper is to develop a methodology for stability analysis of overlapping schemes when interface values are explicitly extrapolated in time with arbitrary accuracy (to allow for temporal consistency in a noniterative case). Our primary concern is to understand the influence of the order of interface extrapolation on stability properties. The analysis is motivated by the fact that implementation of a second- and third-order temporal interface extrapolation in a Navier–Stokes solver resulted in unstable calculations, while a traditional first-order interface scheme remained stable. Since the main focus of the paper is the effect of temporal interface extrapolation on stability, in the current study we have considered a simplified situation of uniformly spaced grids with collocated overlap points. An influence of spatial

interpolation stencil and grid size disparity on stability is an important question and will be considered in future studies.

In this paper, we fix our attention on a purely parabolic problem of an unsteady one-dimensional diffusion equation as it retained (at least qualitatively) peculiar stability properties observed in a Navier–Stokes solver. The current analysis framework, however, is general enough and can be extended to more complicated situations including hyperbolic equations and higher dimensions, as addressed in the discussion section.

The paper is organized as follows. In section 2, we review the existing methods for stability analysis of partial differential equations. In section 3, we present the matrix stability framework, which is applicable for analyzing numerical schemes involving temporal interface extrapolation on overlapping grids, and formulate it for a model problem of a one-dimensional diffusion equation. In section 4, we perform a theoretical analysis of scheme stability and prove the unconditional stability of the first-order extrapolation scheme (EXT1) for the first and second order of time integration (BDF1 and BDF2). In section 5, we explicitly calculate stability thresholds for other (conditionally stable) schemes and show that these thresholds can be increased by invoking iterative loops. In section 6, we present numerical experiments to check the validity of our analysis. In section 7, we look at a semidiscrete equation for the error propagation and confirm the scalings derived for stability bounds in a discrete case. In section 8, we discuss the implication of the current analysis and its extension to more complicated situations.

2. Stability analysis methods. One of the standard methods used to investigate the stability of numerical schemes for partial differential equations is spectral (Fourier) analysis proposed by von Neumann [11], [23]. Although attractive because of its simplicity, von Neumann analysis is limited to uniformly spaced and regular grids. A more general method for stability analysis of time-dependent systems was proposed by Gustaffson, Kreiss, Sundstrøm, and Oliger (the GKSO theory) [13], [14], in which separable normal modes of the solution in the form $u_j^n = z^n \zeta^j$ resulting from a discrete Laplace transform are investigated (ζ^j being a solution to the characteristic equation of the difference scheme). GKSO analysis was used by Berger to investigate the stability of interfaces with mesh and time-step refinement for solving hyperbolic equations on matching grids [1] and by Rivera-Gallego to look at stability properties of an explicit predictor method for solving the heat equation, also on matching grids [31]. The drawback of the GKSO method consists in its difficulty of application, especially to numerical schemes across overlapping subdomains.

A powerful geometrically flexible approach to stability analysis is the method of lines [20] followed by an energy estimate to establish the negativity [5] or, in a more general case of nonnormal systems, coercivity [20] of a spatial operator and to obtain bounds allowing us to choose a stable time step. The specifics of our overlapping grid method with interface temporal extrapolation results, however, in a situation when time dependence is introduced into a spatial operator, and unfortunately the method of lines which considers semidiscrete equations of the form $u_t = L_N u$ is not directly applicable.

Matrix analysis, which consists of investigating the properties of a fully discrete matrix operator for difference equations is therefore a reasonable choice in a situation where discrete equations at every time level contain strong spatiotemporal coupling across multiple layers. Matrix analysis is widely used in analysis of iterative algorithms [9], [40]. For iterative algorithms

$$\mathbf{x}^n = \mathbf{M}\,\mathbf{x}^{n-1}, \tag{2.1}$$

the norm of the error at time n, $\|\mathbf{e}^n\|$, is bounded by

$$\|\mathbf{e}^n\| \leq \|\mathbf{M}\|^n \|\mathbf{e}^0\|, \tag{2.2}$$

where $\|\mathbf{M}\|$ is the corresponding norm of the matrix operator and $\|\mathbf{e}^0\|$ is the norm of the initial error. Behavior of the error in (2.2) depends on the spectral radius of the matrix operator $\rho(\mathbf{M})$ defined as the absolute value of the largest eigenvalue. By the equivalence of norms theorem [9], condition $\rho(\mathbf{M}) < 1$ is the necessary and sufficient condition for $\lim_{n\to 0} \|\mathbf{e}^n\| = 0$ for arbitrary $\|\cdot\|$ and $\|\mathbf{e}^0\|$ and, therefore, for stability of (2.1), since

- $\rho(\mathbf{M}) \leq \|\mathbf{M}\| \ \forall \ \|\cdot\|$;
- for any $\epsilon > 0$, $\exists \|\cdot\|_\star$ such that $\|\mathbf{M}\|_\star \leq \rho(\mathbf{M}) + \epsilon$.

In the rest of the paper, we develop a matrix stability analysis framework suitable for analyzing overlapping grid methods with interface temporal extrapolation of arbitrary accuracy and apply this framework to investigate stability of one-dimensional diffusion equation on overlapping grids.

3. Matrix stability analysis. In this section, we develop a stability analysis framework starting with a discretization scheme and difference equations, followed by a matrix form notation, and finally a stability condition.

3.1. Difference equations. We consider the one-dimensional unsteady diffusion equation

$$\frac{\partial u}{\partial t} - \alpha \frac{\partial^2 u}{\partial x^2} = 0, \ \ x \in (-a, a), \ \ t \in (0, T] \ , \alpha > 0, \tag{3.1}$$

with initial conditions

$$u(x, 0) = u_0(x), \ \ x \in (-a, a) \tag{3.2}$$

and boundary conditions

$$u(-a, t) = u_{-a}(t), \ u(a, t) = u_a(t), t \in [0, T]. \tag{3.3}$$

For the numerical solution of (3.1), the continuous function $u(x, t)$ is discretized in space and time, so that u_j^n represents the value of the corresponding discrete function at the grid point x_j at time level t^n. When the subscript j is omitted, u^n is referred to any numerical value, u_j^n, for any j, at the time level n. Throughout the paper, j, l, m, n, p, q, K, N, and P represent integer numbers. Consider two overlapping subdomains Ω_L and Ω_R, as sketched in Figure 3.1. Assume without loss of generality that the two domains are of equal length L, where $\Omega_L : [-a, \delta/2]$ and $\Omega_R : [-\delta/2, a]$,

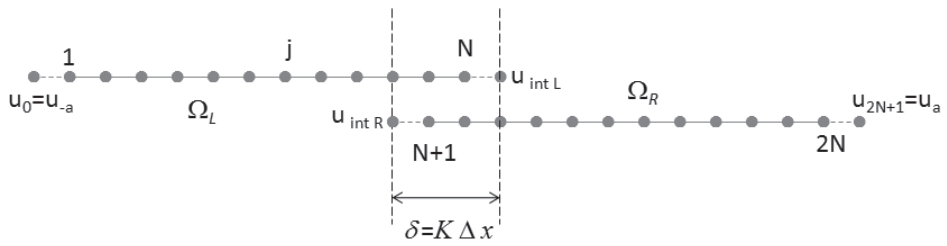

FIG. 3.1. *Two overlapping subdomains in* 1*D.*

TABLE 3.1
Coefficients β_{pl} and γ_{pm} for the BDFl/EXTm schemes, $l = 1, \ldots, 3$, $m = 1, \ldots, 3$.

	$\beta_{p\,1}$	$\beta_{p\,2}$	$\beta_{p\,3}$	$\gamma_{p\,1}$	$\gamma_{p\,2}$	$\gamma_{p\,3}$
$p=0$	1	3/2	11/6			
$p=1$	−1	−2	−3	1	2	3
$p=2$		1/2	3/2		−1	−3
$p=3$			−1/3			1

δ is the size of the overlap, and $L = a + \delta/2$. Assume as well that each subdomain has N interior points, which are numbered with the global indices $j = 1, \ldots, N \in \Omega_L$ and $j = N+1, \ldots, 2\,N \in \Omega_R$. Global indices $j = 0$ and $j = 2\,N+1$ correspond to the left and right boundary points of the composite domain $\Omega_L \cup \Omega_R$, where Dirichlet boundary conditions are specified as $u_0^n = u_{-a}(t^n)$, $u_{2N+1}^n = u_a(t^n)$ according to (3.3). To simplify the theoretical analysis, we avoid interpolation and overlap the grids so that the grid points of Ω_L and Ω_R in $\Omega_L \cap \Omega_R$ coincide. In addition, we assume a uniform distribution of grid points in space and time, $\Delta\,x = \text{const}$ and $\Delta\,t = \text{const}$. The size of the overlap δ can be expressed as $\delta = K\,\Delta\,x$, where K is an integer number equal to the number of shared interior points in each subdomain, $1 \le K \le N$. We will be referring to K as the overlap size throughout the paper. We consider a second-order central difference scheme for discretizing the spatial derivative term in (3.1). Stencils for the points x_N and x_{N+1} require interface conditions to be interpolated from the adjacent subdomain for the interface points, which are the rightmost point of Ω_L and the leftmost point of Ω_R.

For the time advancement, the backward-differentiation scheme (BDF) is considered due to appearance of this scheme in our Navier–Stokes solver [10], [30]. For the BDF scheme of the lth order, the time derivative operator is expressed as

$$D_l \left[\frac{\partial\,u}{\partial\,t}\right]^n = \frac{1}{\Delta\,t}\sum_{p=0}^{l} \beta_{p\,l} u^{n-p}. \tag{3.4}$$

We consider explicit extrapolation for the interface terms (EXT). The extrapolation operator of the mth order is written as follows:

$$E_m\,[u]^n = \sum_{p=1}^{m} \gamma_{p\,m}\,u^{n-p}. \tag{3.5}$$

Coefficients $\beta_{p\,l}$ and $\gamma_{p\,m}$ for the BDFl and EXTm schemes are listed in Table 3.1 for $l = 1, \ldots, 3$, $m = 1, \ldots, 3$. The numerical scheme BDFl/EXTm for solving (3.1) on overlapping grids is as follows:

- Standard stencil, $1 \le j \le 2N$, $j \ne N, N+1$,

$$D_l \left[\frac{\partial\,u}{\partial\,t}\right]_j^n - \alpha\frac{u_{j+1}^n - 2\,u_j^n + u_{j-1}^n}{\Delta\,x^2} = 0; \tag{3.6}$$

- Interface stencil, $j = N$,

$$D_l \left[\frac{\partial\,u}{\partial\,t}\right]_j^n - \alpha\frac{-2\,u_j^n + u_{j-1}^n}{\Delta\,x^2} = \alpha\frac{E_m\,[u]_{int\,L}^n}{\Delta\,x^2}; \tag{3.7}$$

- Interface stencil, $j = N{+}1$,

$$D_l \left[\frac{\partial u}{\partial t}\right]_j^n - \alpha \frac{u_{j+1}^n - 2\,u_j^n}{\Delta x^2} = \alpha \frac{E_m\,[u]_{int\,R}^{\,n}}{\Delta x^2}; \tag{3.8}$$

- Interface conditions

$$E_m\,[u]_{int\,L}^{\,n} = \sum_{p=1}^{m} \gamma_{p\,m}\, u_{N+K}^{n-p},\; E_m\,[u]_{int\,R}^{\,n} = \sum_{p=1}^{m} \gamma_{p\,m}\, u_{N+1-K}^{n-p}. \tag{3.9}$$

3.2. Matrix form. To analyze stability of the numerical scheme (3.6)–(3.9), consider the propagation of errors $z_j^n = u_j^n - u(x_j, t^n)$, where $u(x,t)$ is an exact solution. The error propagation equation can be written in a matrix form followed from (3.6)–(3.9) as

$$\mathbf{A}_l\,\mathbf{z}^n = \sum_{p=1}^{l} \mathbf{B}_{p\,l}\,\mathbf{z}^{n-p} + \sum_{p=1}^{m} \mathbf{C}_{pm}\,\mathbf{z}^{n-p}, \tag{3.10}$$

where $\mathbf{z}^n = \left[z_1^n\; z_2^n\; \ldots\; z_j^n\; \ldots\; z_N^n\; z_{N+1}^n\; \ldots\; z_{2N}^n\right]^T$. Note that the errors at the boundary of the composite domain (z_0^n and z_{2N+1}^n) are identically zero with Dirichlet boundary conditions. Matrices $\mathbf{A}_l$, $\mathbf{B}_{p\,l}$, and $\mathbf{C}_{pm}$ in (3.10) have the following form:

$$\mathbf{A}_l = \beta_{0l}\,\mathbf{I} + \mathbf{Q}, \tag{3.11}$$

$$\mathbf{B}_{p\,l} = -\beta_{p\,l}\,\mathbf{I}, \tag{3.12}$$

$$\mathbf{C}_{p\,m} = \gamma_{p\,m}\,\mathbf{P}_K, \tag{3.13}$$

where matrices $\mathbf{Q}$ and $\mathbf{P}_K$ are defined as

$$\mathbf{Q} = \left[\begin{array}{cccccc|cccccc}
2s & -s & & & & & & & & & & \\
-s & 2s & -s & & & & & & & & & \\
 & \ddots & \ddots & \ddots & & & & & & & & \\
 & & -s & 2s & -s & & & & & & & \\
 & & & -s & 2s & & 0 & & & & & \\
\hline
 & & & & 0 & & 2s & -s & & & & \\
 & & & & & & -s & 2s & -s & & & \\
 & & & & & & & \ddots & \ddots & \ddots & & \\
 & & & & & & & & -s & 2s & -s & \\
 & & & & & & & & & -s & 2s &
\end{array}\right], \tag{3.14}$$

$$\mathbf{P}_K = \left[\begin{array}{cccccccc}
0 & & & & & & & \\
 & \ddots & & & & & & \\
 & & \ddots & \leftarrow & & K & \rightarrow & \\
 & & & 0 & 0 & & s & \\
 & & s & & 0 & 0 & & \\
 & & \leftarrow & K & & \rightarrow & \ddots & \\
 & & & & & & \ddots & \\
 & & & & & & & 0
\end{array}\right], \tag{3.15}$$

$\mathbf{I}$ is the identity matrix, and $s = \alpha\,\Delta t/\Delta x^2$ represents a nondimensional time step, referred to as the stability parameter hereafter. Note that the matrix $\mathbf{P}_K$ depends on the overlap size K. Matrices $\mathbf{A}_l$, $\mathbf{B}_{p\,l}$, $\mathbf{C}_{p\,m}$, $\mathbf{Q}$, and $\mathbf{P}_K$ are $2\,N \times 2\,N$ matrices.

3.3. Stability criteria. Equation (3.10) can be rewritten as

$$\mathbf{z}^n = \sum_{p=1}^{l} \mathbf{A}_l^{-1}\mathbf{B}_{p\,l}\,\mathbf{z}^{n-p} + \sum_{p=1}^{m} \mathbf{A}_l^{-1}\mathbf{C}_{p\,m}\,\mathbf{z}^{n-p} \tag{3.16}$$

and rearranged in the following form:

$$\mathbf{z}^n = \sum_{p=1}^{P} \mathbf{A}_l^{-1}\mathbf{D}_{p\,lm}\mathbf{z}^{n-p}, \tag{3.17}$$

$$\mathbf{D}_{p\,lm} = \left[\Pi(l+1-p)\,\mathbf{B}_{p\,l} + \Pi(m+1-p)\,\mathbf{C}_{p\,m}\right], \tag{3.18}$$

where $P = \max(l, m)$, and $\Pi(x)$ is the "positivity function" defined as

$$\Pi(x) = \begin{cases} 1 & \text{if } x > 0, \\ 0 & \text{if } x \le 0. \end{cases} \tag{3.19}$$

We can analyze stability of a P-level time scheme (3.17) if we write it in the form

$$\left[\mathbf{z}^n\,\mathbf{z}^{n-1}\,\ldots\,\mathbf{z}^{n-P+1}\right]^T = \mathbf{R}_{lm}\,\left[\mathbf{z}^{n-1}\,\mathbf{z}^{n-2}\,\ldots\,\mathbf{z}^{n-P}\right]^T, \tag{3.20}$$

where the discrete matrix $\mathbf{R}_{lm}$ equals to

$$\mathbf{R}_{lm} = \begin{bmatrix} \mathbf{X}_1 & \mathbf{X}_2 & \ldots & \mathbf{X}_{P-1} & \mathbf{X}_P \\ \mathbf{I} & \mathbf{0} & \ldots & \mathbf{0} & \mathbf{0} \\ \mathbf{0} & \mathbf{I} & \ddots & \vdots & \vdots \\ \vdots & \ddots & \ddots & \mathbf{0} & \vdots \\ \mathbf{0} & \ldots & \mathbf{0} & \mathbf{I} & \mathbf{0} \end{bmatrix}, \tag{3.21}$$

and $\mathbf{X}_p = \mathbf{A}_l^{-1}\,\mathbf{D}_{p\,lm}$, $p = 1, \ldots, P$.

A necessary and sufficient condition for the iterative algorithm of (3.20) to be stable is given by [9]

$$\rho\left(\mathbf{R}_{lm}\right) < 1, \tag{3.22}$$

where $\rho(\mathbf{R}_{lm})$ is the spectral radius of the matrix $\mathbf{R}_{lm}$ defined as $\rho(\mathbf{R}_{lm}) = \max_j |\lambda_j(\mathbf{R}_{lm})|$ (λ_j, $j = 1, \ldots, 2NP$, are the eigenvalues of the matrix $\mathbf{R}_{lm}$).

4. Unconditional stability of EXT1 with BDFl, $l = 1, 2$. The developed matrix stability framework can be applied to any BDFl/EXTm scheme by constructing appropriate $\mathbf{R}_{lm}$ matrices and checking if stability condition (3.22) is satisfied. The first important result of this analysis is a strong statement of unconditional stability of the BDF l/EXT1, $l = 1$, 2, scheme for any number of grid points N and any overlap size K. This statement is theoretically proved in the current section.

We begin by first proving the following lemma.

LEMMA 4.1. *For a matrix* $\mathbf{R}_{lm}$ *of* (3.21) *and a number* $\lambda \neq 0$, *the characteristics polynomial* $|\mathbf{R}_{lm} - \lambda\,\mathbf{I}^{(P)}|$ *is equal to*

$$\left|\mathbf{R}_{lm} - \lambda\,\mathbf{I}^{(P)}\right| = \lambda^{2\,N(P-1)}\left|\mathbf{A}_l^{-1}\mathbf{Y} - \lambda\,\mathbf{I}^{(1)}\right|, \tag{4.1}$$

where $\mathbf{I}^{(P)}$ *is a* $2NP \times 2NP$ *identity matrix and* $\mathbf{Y} = \sum_{p=1}^{P} \mathbf{D}_{p\,lm}/\lambda^{p-1}$.

Proof. Matrix $\mathbf{R}_{lm}$ for a P-level time scheme will be referred to as $\mathbf{Z}^{(P)}$. Thus for a one-level time scheme $\mathbf{R}_{lm} = \mathbf{Z}^{(1)}$, for a two-level time scheme $\mathbf{R}_{lm} = \mathbf{Z}^{(2)}$, and so on. Note that for the block matrix $\mathbf{Z}^{(P)} - \lambda\,\mathbf{I}^{(P)}$ one can write (see (3.21)) the following:

$$\mathbf{Z}^{(P)} - \lambda\,\mathbf{I}^{(P)} = \begin{bmatrix} \mathbf{Z}^{(P-1)} - \lambda\,\mathbf{I}^{(P-1)} & \begin{pmatrix} \mathbf{X}_P \\ \mathbf{0} \\ \vdots \\ \mathbf{0} \end{pmatrix} \\ \begin{pmatrix} \mathbf{0} & \dots & \mathbf{0} & \mathbf{I}^{(1)} \end{pmatrix} & -\lambda\,\mathbf{I}^{(1)} \end{bmatrix}. \tag{4.2}$$

Using the formula for the determinant of the block matrices (if $\mathbf{D}$ is nonsingular),

$$\begin{vmatrix} \mathbf{A} & \mathbf{B} \\ \mathbf{C} & \mathbf{D} \end{vmatrix} = |\mathbf{D}|\ \left|\mathbf{A} - \mathbf{B}\,\mathbf{D}^{-1}\mathbf{C}\right|, \tag{4.3}$$

one can write for $\lambda \neq 0$ the following:

$$\left|\mathbf{Z}^{(P)} - \lambda\,\mathbf{I}^{(P)}\right| = \lambda^{2N} \begin{vmatrix} \mathbf{Z}^{(P-2)} - \lambda\,\mathbf{I}^{(P-2)} & \begin{pmatrix} \mathbf{X}_{P-1} + \mathbf{X}_P/\lambda \\ \mathbf{0} \\ \vdots \\ \mathbf{0} \end{pmatrix} \\ \begin{pmatrix} \mathbf{0} & \dots & \mathbf{0} & \mathbf{I}^{(1)} \end{pmatrix} & -\lambda\,\mathbf{I}^{(1)} \end{vmatrix}. \tag{4.4}$$

Applying (4.3) to the right-hand side of (4.4) $P-2$ times, one gets

$$\left|\mathbf{Z}^{(P)} - \lambda\,\mathbf{I}^{(P)}\right| = \lambda^{2N(P-2)} \begin{vmatrix} \mathbf{Z}^{(1)} - \lambda\,\mathbf{I}^{(1)} & \mathbf{X}_2 + \mathbf{X}_3/\lambda + \ldots + \mathbf{X}_P/\lambda^{P-2} \\ \mathbf{I}^{(1)} & -\lambda\,\mathbf{I}^{(1)} \end{vmatrix}, \tag{4.5}$$

which, by the same procedure, reduces to (4.1) and the lemma is proved. ∎

To proceed, we need the following lemma.

LEMMA 4.2. *Let* $\mathbf{A}$ *be a nonsingular matrix. Then the number* λ *is an eigenvalue of the matrix* $\mathbf{A}^{-1}\mathbf{B}$ *if and only if*

$$|\mathbf{B} - \lambda\,\mathbf{A}| = 0. \tag{4.6}$$

Proof. We first prove the necessary statement. Let λ be an eigenvalue of the matrix $\mathbf{A}^{-1}\mathbf{B}$. Then $|\mathbf{A}^{-1}\mathbf{B} - \lambda\,\mathbf{I}| = 0$. We can decompose $|\mathbf{A}^{-1}\mathbf{B} - \lambda\,\mathbf{I}| = |\mathbf{A}^{-1}||\mathbf{B} - \lambda\,\mathbf{A}|$, which for a nonsingular matrix $\mathbf{A}$ proves (4.6).

Now we prove the sufficient statement. Let (4.6) be true. Multiplying both sides of this equation by the determinant of $\mathbf{A}^{-1}$ (which exists and is nonzero, since $\mathbf{A}$ is nonsingular), we get $|\mathbf{A}^{-1}|\ |\mathbf{B} - \lambda\,\mathbf{A}| = \left|\mathbf{A}^{-1}(\mathbf{B} - \lambda\,\mathbf{A})\right| = \left|\mathbf{A}^{-1}\mathbf{B} - \lambda\,\mathbf{I}\right| = 0$, which proves that λ is an eigenvalue of the matrix $\mathbf{A}^{-1}\mathbf{B}$. ∎

The following lemma allows us to cast the analysis of the boundedness of the eigenvalues of the matrix $\mathbf{R}_{lm}$ in a convenient form.

LEMMA 4.3. *If* $\lambda = 1/\mu$ *is a nonzero eigenvalue of the matrix* $\mathbf{R}_{lm}$*, then* $\lambda^\star = F(\mu)$ *is the eigenvalue of the matrix* $\mathbf{S} = \mathbf{A}_l - G(\mu)\,\mathbf{P}_K$*, where* $F(\mu)$ *and* $G(\mu)$ *are*

the polynomials of the form

$$F(\mu) = -\sum_{p=1}^{l} \beta_{p\,l}\,\mu^p, \tag{4.7}$$

$$G(\mu) = \sum_{p=1}^{m} \gamma_{p\,m}\,\mu^p. \tag{4.8}$$

Proof. From Lemma 4.1, $\lambda \neq 0$ is the eigenvalue of the matrix $\mathbf{R}_{l\,m}$ if and only if it is the eigenvalue of the matrix $\mathbf{A}_l^{-1}\mathbf{Y}$, because of the equivalence of the characteristic polynomials, which by Lemma 4.2 implies that $|\mathbf{Y} - \lambda\mathbf{A}_l| = 0$, since $\mathbf{A}_l$ is nonsingular. Using the fact that $\mathbf{Y} = \sum_{p=1}^{P} \mathbf{D}_{p\,l\,m}/\lambda^{p-1}$ and from (3.18), (3.12), and (3.13), we can write matrix $\mathbf{Y}$ as

$$\mathbf{Y} = -\sum_{p=1}^{l} \frac{\beta_{p\,l}}{\lambda^{p-1}}\,\mathbf{I} + \sum_{p=1}^{m} \frac{\gamma_{p\,m}}{\lambda^{p-1}}\,\mathbf{P}_K, \tag{4.9}$$

and we get $|\mathbf{Y} - \lambda\mathbf{A}_l| = 1/\mu^{2N}\,|\mathbf{A}_l - G(\mu)\,\mathbf{P}_K - F(\mu)\,\mathbf{I}| = 0$, which proves that $\lambda^\star = F(\mu)$ is an eigenvalue of the matrix $\mathbf{S} = \mathbf{A}_l - G(\mu)\,\mathbf{P}_K$. ∎

We are now in a position to prove the following important theorem stating the unconditional stability of EXT1 with BDFl, $l = 1, 2$.

THEOREM 1 (stability theorem). *The overlapping scheme with first-order interface extrapolation and the first- and second-order BDF time integration (BDFl/EXT1, $l = 1, 2$) is unconditionally stable for any number of grid points N and any overlap size K.*

Proof. According to the necessary and sufficient stability condition (3.22), the scheme is unconditionally stable if and only if all eigenvalues λ of the matrix $\mathbf{R}_{l\,m}$ satisfy the condition $|\lambda| < 1\ \forall\, s > 0$.

If the matrix $\mathbf{R}_{l\,m}$ has an eigenvalue $\lambda = 0$, it satisfies the condition $|\lambda| < 1$. Now consider nonzero eigenvalues of $\mathbf{R}_{l\,m}$, $\lambda \neq 0$. In this case, one can use Lemma 4.3. According to this lemma the matrix $\mathbf{S} = \mathbf{A}_l - G(\mu)\,\mathbf{P}_K$ has eigenvalues $\lambda^\star$, which are related to the eigenvalues λ of $\mathbf{R}_{l\,m}$ by the relationship $\lambda^\star = F(\mu)$, $\mu = 1/\lambda$.

The matrix $\mathbf{S} = \mathbf{A}_l - G(\mu)\,\mathbf{P}_K$ can be written as (cf. (3.11), (3.14), (3.15))

$$\mathbf{S} = \left[\begin{array}{cccc|cccc}
\beta_{0l}+2s & -s & & & & & & \\
-s & \beta_{0l}+2s & -s & & & & & \\
 & \ddots & \ddots & \ddots & & & & \\
 & & -s & \beta_{0l}+2s & -s & & & \\
 & & & -s & \beta_{0l}+2s & 0 & & -G(\mu)\,s \\
\hline
 & & -G(\mu)\,s & & 0 & \beta_{0l}+2s & -s & \\
 & & & & & -s & \beta_{0l}+2s & -s \\
 & & & & & & \ddots & \ddots \\
 & & & & & & -s & \beta_{0l}+2s
\end{array}\right], \tag{4.10}$$

where the terms $-G(\mu)\,s$ appear in the positions $\mathbf{S}\,(N, N{+}K)$ and $\mathbf{S}\,(N{+}1, N{+}1{-}K)$.

According to Gerschgorin's theorem, the eigenvalues $\lambda^\star$ of $\mathbf{S}$ lie within the union of $2N$ disks

$$|\,\lambda^\star - \mathbf{S}\,(m,m)| \leq \sum_{j\neq m} |\,\mathbf{S}\,(m,j)|\,,\ m = 1, \ldots, 2N. \tag{4.11}$$

Thus, $\lambda^\star$ lies within the union of two sets, $\lambda^\star \in U_1 \bigcup U_2$, where

$$U_1 : |\lambda^\star - (\beta_{0\,l} + 2s)| \leq 2s, \tag{4.12}$$

$$U_2 : |\lambda^\star - (\beta_{0\,l} + 2s)| \leq s(1 + |G(\mu)|). \tag{4.13}$$

The proof proceeds by showing that both sets contain only solutions with $|\lambda| < 1$ for $s > 0$ for EXT1 with BDFl, $l = 1, 2$ schemes, thus proving the unconditional stability of these schemes. Technical details are presented in Appendix A. ∎

5. Stability limits. In the previous section, we proved analytically the unconditional stability of the first-order interface extrapolation scheme with the first- and second-order time integration. The proof cannot be extended to the schemes of order higher than EXT1 or BDF2. To judge about stability of higher-order schemes, we must explicitly estimate the spectral radius of the matrix $\mathbf{R}_{lm}$ and check whether the condition (3.22) is satisfied. In this section, we explicitly evaluate the spectral radius of the matrices $\mathbf{R}_{l\,m}$ for $l = 1, \ldots, 3$, $m = 1, \ldots, 3$ in order to investigate the corresponding scheme stability at a combination of parameters s, K, and N. In addition, we look at the ability of iterations to stabilize the unstable schemes with EXTm, $m > 1$.

5.1. First-order extrapolation schemes. We first look at the dependence of the spectral radius $\rho\,(\mathbf{R}_{l1})$ on the stability parameter s for the first-order extrapolation scheme. The stability theorem guarantees the strict stability of BDF1 and BDF2 schemes with EXT1, so $\rho(\mathbf{R}_{l1})$ is expected to be bounded by unity for any s, K, and N for $l = 1$, 2. Spectral radii of the matrices $\mathbf{R}_{l1}$ are plotted in Figure 5.1 as a function of s for $l = 1, \ldots 3$. One can see from Figure 5.1 that the spectral radii of the matrices $\mathbf{R}_{11}$ and $\mathbf{R}_{21}$ are indeed bounded by unity. Incidentally, the spectral radius of $\mathbf{R}_{31}$ is also bounded by unity for all the parameters investigated. Note that in general we do not expect an unconditional stability of EXT1 with BDF3 or higher, since the stability

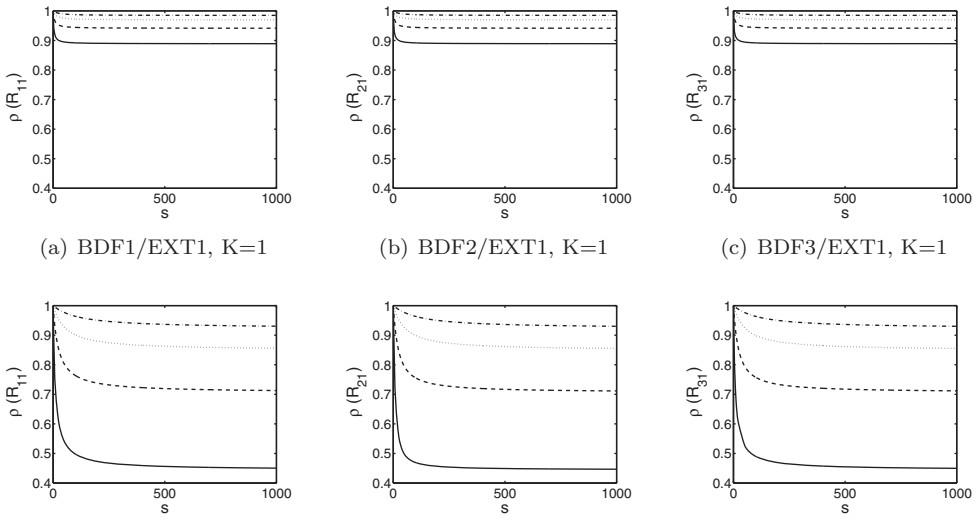

(a) BDF1/EXT1, K=1 (b) BDF2/EXT1, K=1 (c) BDF3/EXT1, K=1

(d) BDF1/EXT1, K=5 (e) BDF2/EXT1, K=5 (f) BDF3/EXT1, K=5

FIG. 5.1. *Spectral radii for the first-order extrapolation and BDF* 1–3. *Solid line,* $N = 8$*; dashed line,* $N = 16$*; dotted line,* $N = 32$*; dash-dotted line,* $N = 64$.

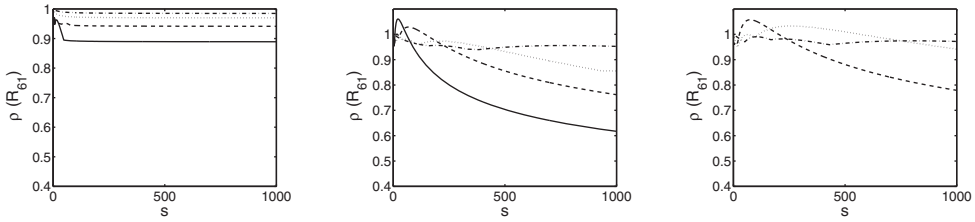

(a) BDF6/EXT1, K=1 (b) BDF6/EXT1, K=5 (c) BDF6/EXT1, K=10

FIG. 5.2. *Spectral radii for the BDF6/EXT1 scheme. Solid line, $N = 8$; dashed line, $N = 16$; dotted line, $N = 32$; dash-dotted line, $N = 64$.*

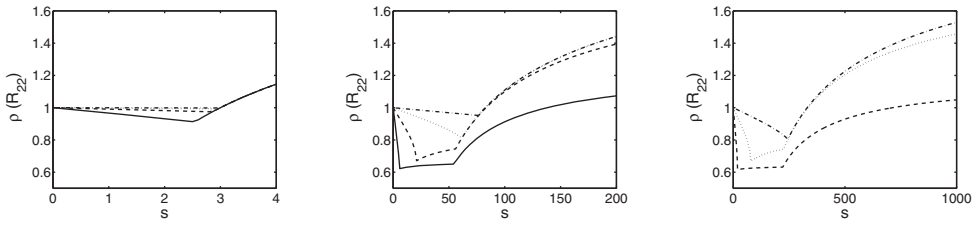

(a) BDF2/EXT2, K=1 (b) BDF2/EXT2, K=5 (c) BDF2/EXT2, K=10

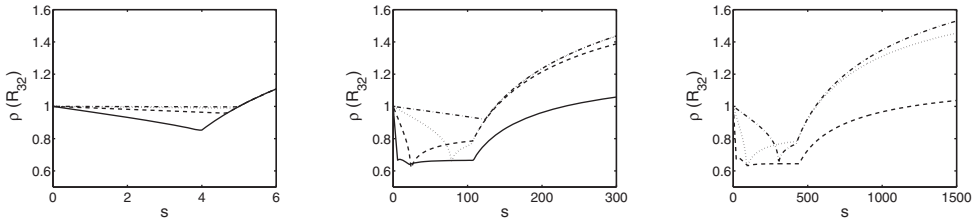

(d) BDF3/EXT2, K=1 (e) BDF3/EXT2, K=5 (f) BDF3/EXT2, K=10

FIG. 5.3. *Spectral radii for the second-order extrapolation. Solid line, $N = 8$; dashed line, $N = 16$; dotted line, $N = 32$; dash-dotted line, $N = 64$.*

theorem cannot be extended to these cases. Indeed, this fact can be demonstrated by Figure 5.2, showing an instability of BDF6/EXT1 at small s for large values of K/N.

5.2. Higher-order extrapolation schemes. We now look at the stability of higher-order extrapolation schemes. We analyze the schemes BDFl/EXTm with $l = 1, \ldots, 3$ and $m = 2, 3$.

5.2.1. Spectral radii. The spectral radii of the matrices $\mathbf{R}_{lm}$ are plotted for $l = 2, 3$ in Figures 5.3 and 5.4 for $m = 2$ and $m = 3$, respectively. One can see that the higher-order extrapolation schemes become unstable with the increase in s. In fact, for any combination of K and N there exists a critical value $s^\star$ such that the method is stable for $s < s^\star$ and unstable for $s \geq s^\star$. We call $s^\star$ a critical stability parameter or stability threshold.

5.2.2. Critical stability parameter. The dependence of critical stability parameter $s^\star$ on the overlap size, K, for a given N is illustrated in Figure 5.5 for the BDFl/EXTm schemes, $l = 1, \ldots, 3$, $m = 2, 3$. One sees from the figures that for each scheme, as long as the relative overlap size K/N is less than a certain value, $s^\star(K)$

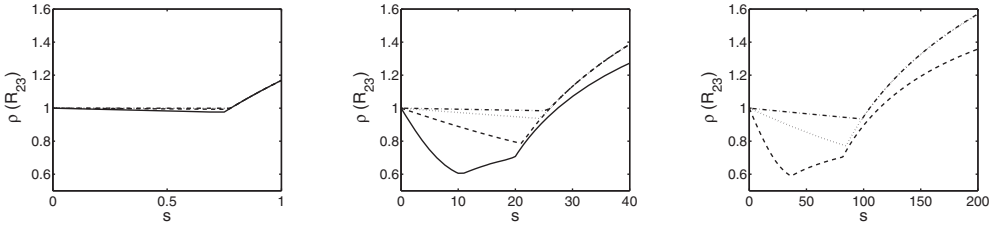

(a) BDF2/EXT3, K=1 (b) BDF2/EXT3, K=5 (c) BDF2/EXT3, K=10

(d) BDF3/EXT3, K=1 (e) BDF3/EXT3, K=5 (f) BDF3/EXT3, K=10

FIG. 5.4. *Spectral radii for the third-order extrapolation. Solid line, $N = 8$; dashed line, $N = 16$; dotted line, $N = 32$; dash-dotted line, $N = 64$.*

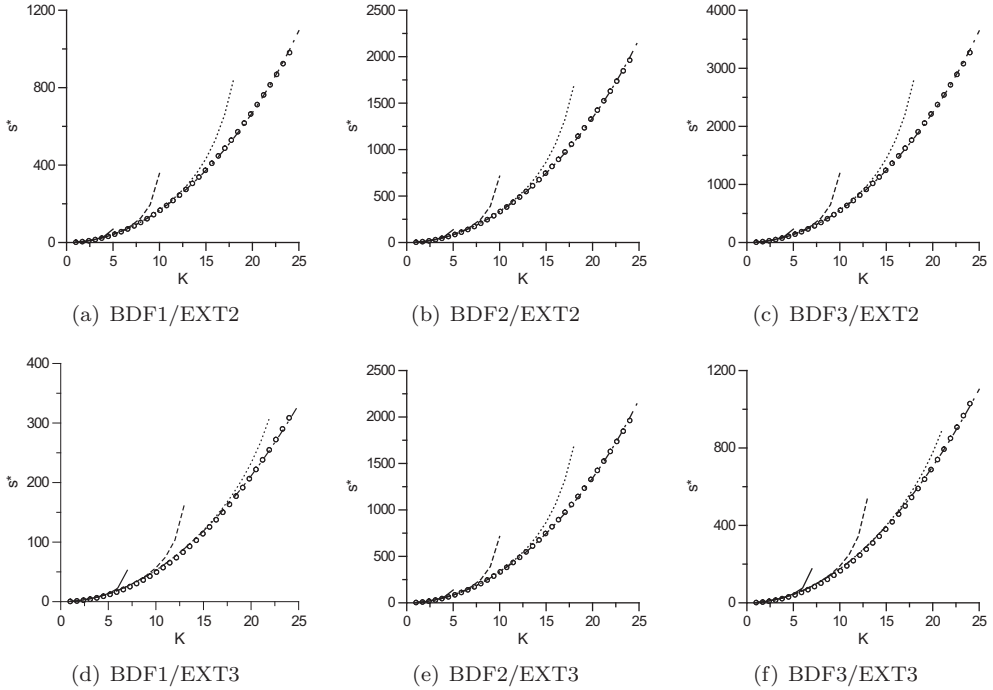

(a) BDF1/EXT2 (b) BDF2/EXT2 (c) BDF3/EXT2

(d) BDF1/EXT3 (e) BDF2/EXT3 (f) BDF3/EXT3

FIG. 5.5. *Dependence of critical value $s^\star$ on the overlap size K. Solid line, $N = 8$; dashed line, $N = 16$; dotted line, $N = 32$; dash-dotted line, $N = 64$; circles correspond to empirical fit $s^\star(K) = s_0^\star K^2$ with parameters from Table* 5.1.

TABLE 5.1
Value of $s_0^\star$ for the empirical fit $s^\star(K)$ of (5.1) for the BDFl/EXTm schemes.

Scheme	$s_0^\star$		
	BDF1	BDF2	BDF3
EXT2	1.5	3	5
EXT3	0.39	0.78	1.3

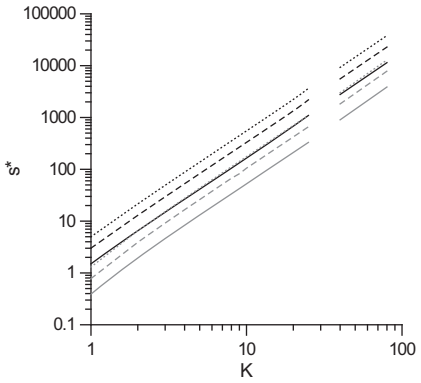

FIG. 5.6. *Dependence of stability limit $s^\star$ on the number of overlapping points K in log-log scale, $N = 64$. Black lines, second-order extrapolation; gray lines, third-order extrapolation. Solid lines, BDF1; dashed lines, BDF2; dotted lines, BDF3; curves to the right correspond to the empirical fit of (5.1).*

plots fall on the same curve independent of N, which can be described by an empirical power law

$$s^\star(K) \sim s_0^\star K^2, \tag{5.1}$$

where $s_0^\star$ corresponds to the stability limit with the minimum overlap $K = 1$. Values of $s_0^\star$ in the power law providing the best fit are summarized in Table 5.1. Figure 5.6 shows this dependence in a log-log scale, where actual stability limits are plotted alongside the empirical curves of (5.1) for $N = 64$ for different schemes. We will show later in the paper that in a semidiscrete case an analogous quadratic scaling $\Delta t^\star \sim (s_0^\star/\alpha)\,\delta^2$ can be derived for small overlap sizes.

5.2.3. Critical overlap size. To determine the critical overlap size for which the scaling of (5.1) is valid, we plot the value of $s^\star$ versus the number of grid points N for a constant K in Figure 5.7. It is seen that the critical overlap size value is $K/N \sim 1/2$. When $K/N < 1/2$, an asymptotic behavior of (5.1) independent of N is recovered; when $K/N > 1/2$, the stability curves deviate rapidly from the asymptotic value.

5.2.4. Stability regimes. The current analysis shows that there are two stability regimes. When the relative overlap size is small ($K/N < 1/2$; the overlap is less than half a subdomain), the stability limit increases quadratically with K. However, when the relative overlap is sufficiently large ($K/N > 1/2$), further increase of overlap leads to an increase in the stability threshold with a much higher rate. In practice, that would be the desired goal for stability; however, a large overlap size also increases the computational expenses per time step, so that an appropriate compromise must

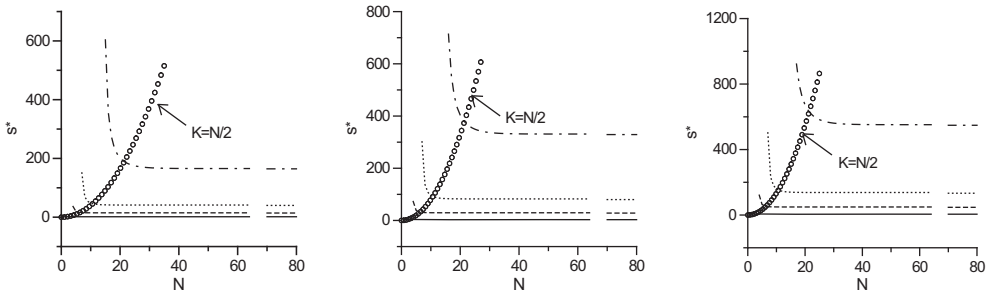

(a) BDF1/EXT2 (b) BDF2/EXT2 (c) BDF3/EXT2

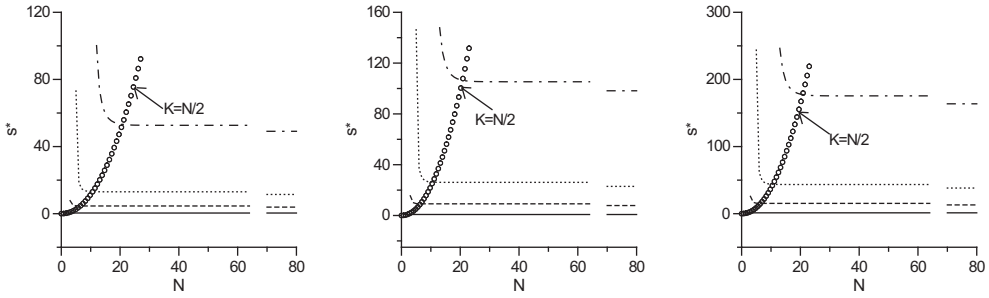

(d) BDF1/EXT3 (e) BDF2/EXT3 (f) BDF3/EXT3

FIG. 5.7. *Dependence of stability limit $s^\star$ on the number of grid points N. Solid line, $K = 1$; dashed line, $K = 3$; dotted line, $K = 5$; dash-dotted line, $K = 10$; lines to the right correspond to the empirical fit of* (5.1) *for the given value of K; circles correspond to* (5.1) *with $K = N/2$.*

be found. In addition, the overlap size in practice is often limited by geometrical or physical constraints.

5.2.5. Scheme ranking with respect to stability. Equation (5.1), Table 5.1, and Figure 5.6 show that stability limits are the lowest for the BDF1 scheme and increase with the order of accuracy, so that the first-order scheme is the least stable and the third-order scheme is the most stable for the same interface conditions. On the other hand, increasing the order of interface extrapolation destabilizes the scheme. Thus, BDF1/EXT2 has similar stability limits as BDF3/EXT3, while BDF3/EXT2 appears to be the most stable scheme and BDF1/EXT3 the least stable scheme of those investigated.

5.2.6. Summary. Due to complexity of the problem and influence of at least two parameters, such as physical overlap size, K, and relative overlap size, K/N, on stability, a simple representation of stability limits (such as a single number for each scheme) is not possible. The most complete representation of stability results is given by Figure 5.5, showing the dependence of stability limits $s^\star$ on K for different N and different schemes. For small overlap sizes, only one parameter becomes important, and stability results are best indicated by (5.1), together with Table 5.1 (see also Figure 5.6).

5.3. Influence of iterations. Numerical experiments showed that the stability properties of higher-order extrapolation schemes can be improved significantly by invoking an iterative loop. In this section, we show how to incorporate the pres-

ence of iterations into the developed stability framework and analyze the influence of iterations on stability.

If an iterative loop is introduced into the numerical scheme (3.6)–(3.9), the scheme becomes the following:

- Standard stencil, $1 \le j \le 2N$, $j \ne N, N+1$,

$$\tilde{D}_l \left[\frac{\partial u}{\partial t}\right]_j^{q,n} - \alpha \frac{u_{j+1}^{q,n} - 2\,u_j^{q,n} + u_{j-1}^{q,n}}{\Delta x^2} = 0; \tag{5.2}$$

- Interface stencil, $j = N$,

$$\tilde{D}_l \left[\frac{\partial u}{\partial t}\right]_j^{q,n} - \alpha \frac{-2\,u_j^{q,n} + u_{j-1}^{q,n}}{\Delta x^2} = \alpha \frac{E_m\,[u]_{int\,L}^{q,n}}{\Delta x^2}; \tag{5.3}$$

- Interface stencil, $j = N+1$,

$$\tilde{D}_l \left[\frac{\partial u}{\partial t}\right]_j^{q,n} - \alpha \frac{u_{j+1}^{q,n} - 2\,u_j^{q,n}}{\Delta x^2} = \alpha \frac{E_m\,[u]_{int\,R}^{q,n}}{\Delta x^2}; \tag{5.4}$$

- Interface conditions,

$$q = 1:\ E_m\,[u]_{int\,L}^{q,n} = \textstyle\sum_{p=1}^{m} \gamma_{p\,m}\,u_{N+K}^{n-p},\ E_m\,[u]_{int\,R}^{q,n} = \sum_{p=1}^{m} \gamma_{p\,m}\,u_{N+1-K}^{n-p},$$

$$q > 1:\ E_m\,[u]_{int\,L}^{q,n} = u_{N+K}^{q-1,n},\ E_m\,[u]_{int\,R}^{q,n} = u_{N+1-K}^{q-1,n}.$$

In addition, $u^{0,n} = u^{n-1}$, $u^n = u^{qmax,n}$. Here $q = 1, \ldots, qmax$ is the iteration number, and $qmax$ is the maximum number of iterations. The time derivative operator $\tilde{D}_l$ for the iterative schemes is slightly modified from its noniterative counterpart of (3.4):

$$\tilde{D}_l \left[\frac{\partial u}{\partial t}\right]^{q,n} = \frac{1}{\Delta t}\left(\beta_{0\,l}\,u^{q,n} + \sum_{p=1}^{l} \beta_{p\,l}\,u^{n-p}\right). \tag{5.5}$$

One can see that for $qmax = 1$, one recovers the original noniterative scheme (3.6)–(3.9). Since the noniterative scheme is unconditionally stable for $m = 1$, $l = 1, 2$, and stable for at least $s \le 10^3$ for $l = 3, \ldots, 5$, we will consider only $m = 2, 3$ for iterative schemes.

5.3.1. Matrix form with iterations. To cast (5.2)–(5.5) into the matrix form, we can write for the error $z_j^n = u_j^n - u(x_j, t^n)$, analogously to (3.17),

$$\begin{aligned} \mathbf{z}^{q,n} &= \sum_{p=1}^{P} \mathbf{A}_l^{-1}\mathbf{D}_{p\,lm}\mathbf{z}^{n-p},\ q = 1, \\ \mathbf{z}^{q,n} &= \sum_{p=1}^{l} \mathbf{A}_l^{-1}\mathbf{B}_{p\,l}\mathbf{z}^{n-p} + \mathbf{A}_l^{-1}\mathbf{C}_{11}\mathbf{z}^{q-1,n},\ q > 1. \end{aligned} \tag{5.6}$$

Equations (5.6) can be further rewritten as

$$\begin{aligned} \left[\mathbf{z}^{1,n}\,\mathbf{z}^{n-1}\ \ldots\ \mathbf{z}^{n-P}\right]^T &= \mathbf{T}_1\ \left[\mathbf{z}^{n-1}\,\mathbf{z}^{n-2}\ \ldots\ \mathbf{z}^{n-P-1}\right]^T,\ q = 1; \\ \left[\mathbf{z}^{q,n}\,\mathbf{z}^{n-1}\ \ldots\ \mathbf{z}^{n-P}\right]^T &= \mathbf{T}_q\ \left[\mathbf{z}^{q-1,n}\,\mathbf{z}^{n-1}\ \ldots\ \mathbf{z}^{n-P}\right]^T,\ q > 1; \end{aligned} \tag{5.7}$$

$$\mathbf{T}_1 = \begin{bmatrix} \mathbf{A}_l^{-1}\mathbf{D}_{1\,lm} & \mathbf{A}_l^{-1}\mathbf{D}_{2\,lm} & \dots & \mathbf{A}_l^{-1}\mathbf{D}_{P\,lm} & \mathbf{0} \\ \mathbf{I} & \mathbf{0} & \dots & \mathbf{0} & \vdots \\ \mathbf{0} & \mathbf{I} & \ddots & \vdots & \vdots \\ \vdots & \ddots & \ddots & \mathbf{0} & \vdots \\ \mathbf{0} & \dots & \mathbf{0} & \mathbf{I} & \mathbf{0} \end{bmatrix}; \tag{5.8}$$

$$\mathbf{T}_q = \left[\begin{array}{ccccc|ccc} \mathbf{A}_l^{-1}\mathbf{C_{11}} & \mathbf{A}_l^{-1}\mathbf{B}_{1\,l} & \mathbf{A}_l^{-1}\mathbf{B}_{2\,l} & \dots & \mathbf{A}_l^{-1}\mathbf{B}_{l\,l} & \mathbf{0} & \dots & \mathbf{0} \\ \mathbf{0} & \mathbf{I} & \mathbf{0} & \dots & \mathbf{0} & \vdots & \ddots & \vdots \\ \vdots & \mathbf{0} & \ddots & \ddots & \vdots & \vdots & \ddots & \vdots \\ \vdots & \ddots & \ddots & \ddots & \mathbf{0} & \vdots & \ddots & \vdots \\ \vdots & \ddots & \ddots & \ddots & \mathbf{I} & \mathbf{0} & \ddots & \vdots \\ \vdots & \ddots & \ddots & \ddots & \mathbf{0} & \mathbf{I} & \ddots & \vdots \\ \vdots & \ddots & \ddots & \ddots & \vdots & \mathbf{0} & \ddots & \mathbf{0} \\ \mathbf{0} & \dots & \dots & \dots & \mathbf{0} & \dots & \mathbf{0} & \mathbf{I} \end{array}\right], q > 1. \tag{5.9}$$

All the matrices T_1 through T_{qmax} are $(P+1)\times(P+1)$ block matrices, each block of size $2N \times 2N$. Additional $m-l$ block columns appear at the right of the matrix $T_q, q>1$, if $m<l$. From the fact $\mathbf{z}^{qmax,n} = \mathbf{z}^n$ it follows from (5.7) that

$$\left[\mathbf{z}^n\, \mathbf{z}^{n-1}\, \dots\, \mathbf{z}^{n-P}\right]^T = \mathbf{T}\, \left[\mathbf{z}^{n-1}\, \mathbf{z}^{n-2}\, \dots\, \mathbf{z}^{n-P-1}\right]^T, \tag{5.10}$$

where $\mathbf{T} = \mathbf{T}_{qmax} \dots \mathbf{T}_2\, \mathbf{T}_1$. The stability condition for the iterative schemes is $\rho(\mathbf{T}) < 1$.

5.3.2. Stability limits with iterations. The spectral radius $\rho(\mathbf{T})$ for different numbers of iterations $qmax = 1, \dots, 4$ is plotted in Figure 5.8 for the BDFl/EXTm schemes with $l = 2, 3$, $m = 2, 3$, for $N = 32$ and $K = 5$. Note that $qmax = 1$ corresponds to the noniterative scheme. As expected, the effect of iterations is to reduce the spectral radius and increase the stability limit. The number of iterations sufficient to stabilize the scheme for a given s is plotted in Figures 5.9 and 5.10 for EXT2 and EXT3, respectively. Clearly, it is easier to stabilize the schemes with the large values of K. The number of iterations $qmax$ decreases significantly with the increase in K, and it also decreases with the decrease in N. Moreover, the higher-order time integration and the lower-order interface extrapolation require fewer iterations to

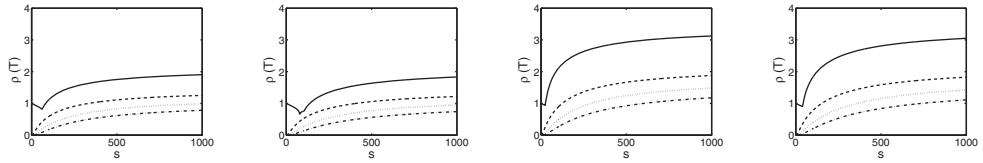

(a) BDF2/EXT2 (b) BDF3/EXT2 (c) BDF2/EXT3 (d) BDF3/EXT3

FIG. 5.8. *Spectral radii for the schemes with iterations.* $N = 32$, $K = 5$. *Solid line,* $qmax = 1$*; dashed line,* $qmax = 2$*; dotted line,* $qmax = 3$*; dash-dotted line,* $qmax = 4$.

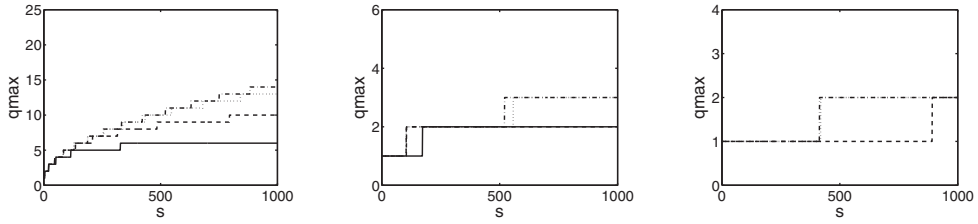

(a) BDF2/EXT2, K=1 (b) BDF2/EXT2, K=5 (c) BDF2/EXT2, K=10

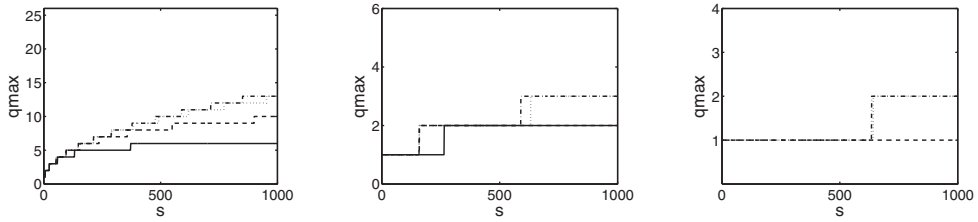

(d) BDF3/EXT2, K=1 (e) BDF3/EXT2, K=5 (f) BDF3/EXT2, K=10

FIG. 5.9. *Number of iterations sufficient to stabilize the scheme for the second-order extrapolation. Solid line, $N = 8$; dashed line, $N = 16$; dotted line, $N = 32$; dash-dotted line, $N = 64$.*

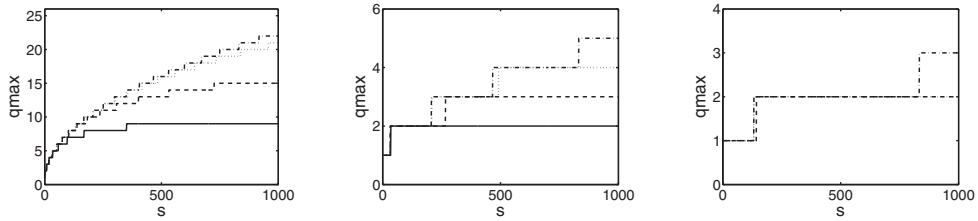

(a) BDF2/EXT3, K=1 (b) BDF2/EXT3, K=5 (c) BDF2/EXT3, K=10

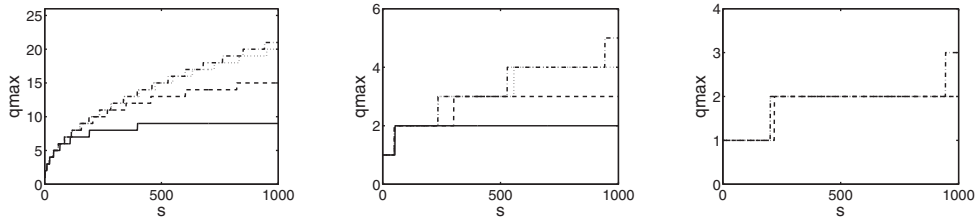

(d) BDF3/EXT3, K=1 (e) BDF3/EXT3, K=5 (f) BDF3/EXT3, K=10

FIG. 5.10. *Number of iterations sufficient to stabilize the scheme for the third-order extrapolation. Solid line, $N = 8$; dashed line, $N = 16$; dotted line, $N = 32$; dash-dotted line, $N = 64$.*

be stable, consistent with the previous conclusions. For $K = 5$, two to five iterations are sufficient for all the schemes investigated. For $K = 10$, a maximum of three iterations is required.

6. Numerical experiments. We check the obtained stability bounds by solving (3.1) numerically in a domain $x \in [-a, a]$ with initial conditions $u(x, 0) = \cos(\pi x/2)$ and Dirichlet boundary conditions $u(\pm a, t) = \cos(\pi a/2)\, e^{-\alpha\pi^2 t/4}$, which has an exact

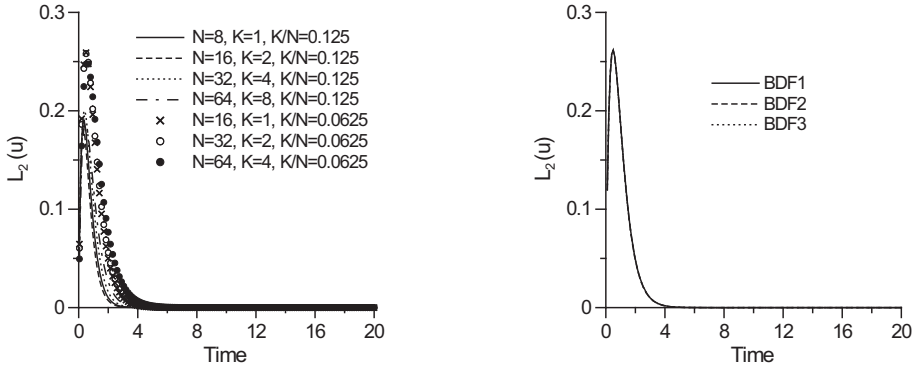

(a) BDF1/EXT1 with different values of K and N.

(b) Dependence on the BDF order, EXT1 scheme, $N = 32, K = 5$.

FIG. 6.1. *$L_2(u)$ error versus computational time, $s = 10^3$.*

solution $u(x,t) = \cos(\pi x/2)\, e^{-\alpha\pi^2 t/4}$. We set the grid resolution to be $\Delta x = 0.01$ for all the calculations. The overlap size K and the number of grid points in each subdomain N are the input parameters. The physical overlap size δ is then determined as $\delta = K\Delta x$, the length of each subdomain as $L = (N+1)\Delta x$, and $a = (N + 1 - K/2)\Delta x$. Unconditional stability of the EXT1 scheme for $l = 1, 2$ can be demonstrated by plotting the L_2 error between the numerical and exact solution $L_2(u) = \sqrt{\sum_{j=1}^{2N}[u_j^n - u(x_j, t^n)]^2/(2N)}$ versus time for $s = 10^3$; see Figure 6.1. Although accuracy analysis is not the subject of the present paper, the relative overlap size K/N might be a relevant parameter in that matter. Dependence of the error on the BDF order for EXT1 is investigated in Figure 6.1(b) for $N = 32$, $K = 5$. The errors are not influenced by the BDF order in a stable regime, since the temporal error is dictated by the first-order temporal accuracy of the interface extrapolation, so that increasing the order of integration does not lead to the error reduction. (Spatial errors are the same because of a fixed grid resolution $\Delta x = 0.01$.)

For the order of interface extrapolation higher than 1, one would expect an unstable behavior, according to the previous analysis. This was indeed confirmed by the numerical experiments: the calculations with EXT2 and EXT3 were stable for $s < s^{\star\, n}$ and unstable for $s \geq s^{\star\, n}$. Comparison of the theoretical values of $s^\star$ with the values $s^{\star\, n}$ observed in the calculations is given in Table 6.1 for $K = 5$; the schemes are listed in the order of least stable to most stable. One can see that the computed stability thresholds are fairly close to the theoretical limits and, most important, they never fall below the theoretical values. Calculated thresholds $s^{\star\, n}$ sometimes exceed the theoretical values $s^\star$ due to the fact that numerical perturbations can be too small to trigger the instability for the values of $s \in [s^\star, s^{\star\, n})$, especially for large relative overlap sizes, K/N, for which the errors are the smallest (see Figure 6.1).

The drastic change in the scheme behavior when the stability threshold is crossed is demonstrated in Figure 6.2(a), where $L_2(u)$ error is plotted versus time for the BDF3/EXT3 scheme with $N = 32$, $K = 5$ for s slightly smaller than $s^{\star\, n}$ ($s = 42.5$, $s^{\star\, n} = 43$) and slightly larger than $s^{\star\, n}$ ($s = 43.5$, $s^{\star\, n} = 43$). The beginning of the instability is clearly seen. The stabilizing influence of the iterations is demonstrated in Figure 6.2(b), where the $L_2(u)$ error is plotted versus the computational time for the same case but with $s = 200$. The calculations with one iteration are unstable, while the calculations with two iterations are stable, consistent with Figure 5.10(e).

TABLE 6.1
Comparison of the theoretical values of $s^\star$ with the numerical values $s^{\star\, n}$, $K = 5$.

Scheme	$N = 8$	$N = 16$	$N = 32$	$N = 64$
	$s^\star / s^{\star\, n}$			
BDF1/EXT3	14/20	13/19	13/13	13/13
BDF2/EXT3	27/41	26/39	26/26	26/26
BDF3/EXT3	46/70	43/70	43/43	43/43
BDF1/EXT2	69/100	42/70	41/49	41/49
BDF2/EXT2	138/190	83/122	82/100	82/100
BDF3/EXT2	230/300	139/200	138/160	138/160

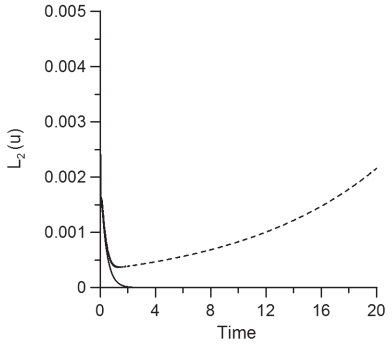

(a) Solid line, $s < s^{\star\, n}$ ($s = 42.5$, $s^{\star\, n} = 43$); dashed line, $s > s^{\star\, n}$ ($s = 43.5$, $s^{\star\, n} = 43$)

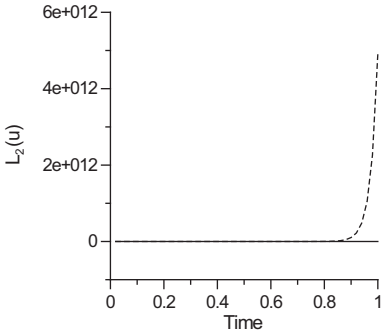

(b) Dashed line, 1 iteration; solid line, 2 iterations; $s = 200$.

FIG. 6.2. *$L_2(u)$ error versus computational time for BDF3/EXT3 scheme with $N = 32$, $K = 5$.*

7. Semidiscrete analysis. The above-mentioned stability properties were derived for a central difference spatial discretization of a second-derivative term. However, similar stability behavior was observed for different spatial discretization schemes, such as spectral elements [10]. It is likely that the observed stability characteristics are related to temporal discretization and are somewhat independent of a spatial scheme. To confirm that hypothesis, we performed a stability analysis of the corresponding semidiscrete equation governing the error propagation, similar to the analysis of the rate of convergence of the overlapping Schwarz methods [9]. We found that the quadratic dependence of the stability limit on the overlap size K for small overlaps given by (5.1), as well as unconditional stability of the EXT1 scheme, can be derived asymptotically from a semidiscrete equation. Indeed, it can be shown (see Appendix B) that in a semidiscrete case the stability bound of a BDFl/EXTm scheme is

$$\Delta t < \frac{s_0^\star}{\alpha}\,\delta^2, \quad s_0^\star = \frac{\beta_{0\,l}}{\ln^2(\gamma_{1\,m})}, \tag{7.1}$$

which is a semidiscrete analogue to a quadratic stability bound $s < s_0^\star K^2$ of (5.1).

Thus, asymptotic semidiscrete analysis not only confirms the quadratic dependence of Δt on the overlap size δ for small overlap regions but also gives the correct trend of increasing stability limit with the order of the BDF scheme ($\beta_{0\,l}$) and decreasing with the order of the EXT scheme ($\gamma_{1\,m}$); cf. (7.1) with Table 5.1. Note

that Dawson, Du, and Dupont [8] also reported a similar quadratic stability bound $\Delta t < H^2/2$ independent of Δx for their patched multidomain solution of the heat equation, where H was the parameter defining the stencil for an explicit interface update, analogous to the overlap size in our scheme.

8. Discussion.

8.1. Diffusion equation. In the present paper, we have developed a matrix framework for stability analysis of numerical schemes on overlapping grids that employ temporal extrapolation of interface terms of order m (EXTm). We have used the developed framework to analyze the stability properties of BDFl/EXTm schemes applied to a one-dimensional diffusion equation. Our findings with respect to stability properties of this class of schemes are as follows:

- First-order interface extrapolation (EXT1) with first- and second-order time integration (BDF1, BDF2) is unconditionally stable for any number of grid points and any overlap size, as theoretically proved in section 4.
- It was shown by explicitly evaluating matrix eigenvalues that the time integration schemes up to fifth order with EXT1 retain the stability properties of the lower-order schemes for the range of parameters investigated, while the sixth-order BDF scheme with EXT1 was found unstable for large values of K/N for the same range of parameters.
- For higher-order interface extrapolation (EXTm, $m > 1$), the numerical schemes become unstable as the time step (equivalently, stability parameter s) increases. By evaluating the spectral radius for increasing values of s, we have established the critical stability conditions for the BDFl/EXTm schemes with $l = 1, \ldots, 3$, $m = 2, 3$. We discovered that the stability limit increases quadratically with the size of the overlap K as long as $K/N < 1/2$, and with a much higher rate when $K/N > 1/2$.
- Semidiscrete analysis confirms the observed properties of quadratic dependence of the stability limit on the overlap size, as well as the unconditional stability of the EXT1 scheme for small overlaps, thus showing that the derived stability characteristics are the consequence of the temporal discretization and are somewhat independent of spatial discretization of a second-derivative term.
- It was also found that the stability limit can increase significantly if an iterative loop is invoked. In practice, for reasonable overlap sizes ($K \geq 5$) and number of grid points ($N \leq 64$), two to five iterations are sufficient to completely stabilize the scheme for the nondimensional time step $s = \alpha \Delta t/\Delta x^2$ at least as big as 10^3.
- Numerical experiments confirm the theoretical conclusions.

The question was raised in the introduction about the utility of Schwarz iterations with overlapping schemes. From the previous discussion, we have established that Schwarz iterations are beneficial for stability or accuracy considerations, or both. We have also commented that they are not required from the accuracy standpoint for the "consistent" schemes [43] (schemes where the difference between physical quantities due to interface conditions is of the same order of accuracy as that of the overall solution method). With this definition, BDFl/EXTm with $m \geq l$ would be considered consistent, but in practice it is more suitable to use BDFl/EXTl schemes, since increasing the interface conditions accuracy beyond the time integration accuracy is associated with extra costs and does not increase the overall accuracy of the scheme.

The findings in this paper allow us to make two important conclusions concerning practical use of consistent numerical schemes on overlapping grids for parabolic equations and necessity of Schwarz iterations.

The first conclusion is that the first-order accuracy consistent scheme, BDF1/EXT1, is unconditionally stable without iterations. Therefore, one can obtain a strictly stable and computationally efficient first-order scheme without the need for Schwarz iterations.

The second conclusion is that higher-order schemes, BDF2/EXT2 and higher, are not unconditionally stable. To use them, one can either choose a time step below the critical value (note that stability bounds dictated by the observed "parabolic" instability are generally quite high and not restrictive) or stabilize the scheme with iterations at any time step (as analysis in this paper shows, in most cases the scheme can be stabilized with two to five iterations). Both these strategies are more efficient than employing BDFl with EXT1 (unconditionally stable) and using Schwarz iterations *until convergence* to increase the accuracy to that of a consistent scheme. As discussed earlier, driving Schwarz iterations to convergence can be an expensive procedure, sometimes requiring tens or hundreds of iterations [39], and is not justifiable.

8.2. Implication for Navier–Stokes equations. The developed matrix stability analysis framework is generally extendable to more complicated situations, including hyperbolic equations, nonuniform grids, presence of spatial interpolation operators, and higher dimensions, by modifying the coefficient matrices corresponding to new discrete relations. Extension to nonlinear equations is also possible by the method of frozen coefficients [20], [23].

An interesting question is how the stability properties change when a convective term is added to the diffusion equation and it becomes more and more hyperbolic, since this situation is more representative of true Navier–Stokes equations. To answer this question, we have investigated stability properties of a purely hyperbolic advection equation $\partial u/\partial t + a\,\partial u/\partial x = 0$.

A general answer is that stability properties of an advection equation solved on overlapping grids with BDFl/EXTm scheme largely depend on a convective term discretization. Thus, for upwind discretization of a convective term, stability properties of the underlying single-grid scheme do not change with the addition of overlapping grids. BDF schemes with a convective term treated implicitly (unconditionally stable for a single grid for BDFl, $l = 1, 3$) remain unconditionally stable with overlapping grids with EXTm, $m = 1, 3$. BDF schemes with a convective term treated explicitly (stable under appropriate time-step constraint) remain stable under the same time-step constraint with overlapping grids. However, BDF schemes with a convective term treated with a central scheme (implicitly, since the explicit central scheme is always unstable on a single grid) exhibit completely different behavior. Note that even an implicit central scheme can be unstable on a single grid for BDF3 at $C_a < C^\star$ and stable for $C_a > C^\star$ ($C_a = a\,\Delta t/\Delta x$), opposite a "conventional" stability behavior, due to the presence of purely imaginary eigenvalues (BDF1, 2 are unconditionally stable on a single grid) [9]. In the presence of overlapping grids, all BDFl, $l = 1, 3$, schemes exhibit the similar behavior of being unstable for $C_a < C^\star$ and stable for $C_a > C^\star$ for EXTm, $m = 1, 3$. Stability limit $C^\star$ depends on numerical parameters and can reach up to fairly large values ($C^\star > 10^3$ for some schemes at small overlaps), making the central scheme not an ideal choice for solving hyperbolic equations, especially on overlapping grids. Stability conditions derived for linear hyperbolic equations can be extended to nonlinear equations by bounding $C_U = U\Delta t/\Delta x < C^\star$, where $U = \max u$.

What happens with the advection-diffusion equation depends largely on the relative importance of convective to diffusive terms determined by Péclet ($Pe = U\,L/\alpha$) or Reynolds ($Re = U\,L/\nu$) number. It was observed that at small Péclet numbers ($Pe \prec 10$), viscous (parabolic) stability would dominate, and at large Péclet numbers ($Pe \succ 1000$), convective (hyperbolic) stability would play a role. At intermediate Péclet numbers, both instabilities counteract, and the overall pattern is more complex. The diffusion-dominated situation investigated in the current paper would thus fall into a low-Reynolds-number regime for Navier–Stokes equations. As mentioned in the introduction, the instability of second- and third-order temporal interface extrapolation schemes and complete robustness of the first-order scheme was observed in a spectral element Navier–Stokes solver [10] at low Reynolds number $Re \sim 10$. At higher Reynolds numbers the situation might change, and further studies are required to relate behavior of Navier–Stokes equations discretized on overlapping grids to theory in a more advection-dominated regime.

Appendix A. Stability theorem. In this appendix, we present the algebra involved in proving Theorem 1 (stability theorem). In particular, we show that the sets U_1 and U_2 given by (4.12) and (4.13) contain only the eigenvalues satisfying $|\lambda| < 1$ for $s > 0$ for EXT1 with BDFl, $l = 1, 2$.

Set U_1. Let us first consider the set U_1 given by condition (4.12). In what follows, we prove that this condition implies, for $s > 0$, $|\mu| > 1$ or $|\lambda| < 1$.

Condition (4.12) means that $\lambda^\star$ lies inside the disk with the center at $\beta_{0\,l} + 2s$ and the radius of $2s$. Therefore,

$$Re(\lambda^\star) \geq \beta_{0\,l}, \tag{A.1}$$

where $Re(\lambda^\star)$ denotes the real part of $\lambda^\star$. Equality occurs when $s = 0$. Since $\lambda^\star = F(\mu)$, (A.1) for $s > 0$ is equivalent to

$$Re\,\{H(\mu)\} < 0, \tag{A.2}$$

where

$$H(\mu) = \beta_{0\,l} - F(\mu) = \sum_{p=0}^{l} \beta_{p\,l}\,\mu^p \tag{A.3}$$

(cf. (4.7)). We will prove that (A.2) implies $|\mu| > 1$ for BDFl, $l = 1, 2$, that is, if $|\mu| \leq 1$, then $Re\,\{H(\mu)\} \geq 0$.

Consider the complex number μ in the exponential form $\mu = r\,e^{i\phi}$. Then $Re\,\{H(\mu)\}$ can be written as

$$Re\,\{H(\mu)\} = \sum_{p=0}^{l} \beta_{p\,l}\,r^p\,\cos\,(p\,\phi). \tag{A.4}$$

We can write $Re\,\{H(\mu)\}$ as a polynomial of $\xi = \cos(\phi)$ as

$$Re\,\{H(\mu)\} = \sum_{p=0}^{l} \tilde{\beta}_{p\,l}(r)\,\xi^p, \tag{A.5}$$

where the polynomials $\tilde{\beta}_{p\,l}(r)$ can be obtained from the coefficients $\beta_{p\,l}$ and the powers of r by using the corresponding multiple-angle formulas for $\cos(p\,\phi)$. Now let us

consider the complex numbers μ lying on the unit circle ($|\mu| = 1$):

$$Re\,\{H(\mu)\}_{|\mu|=1} = \sum_{p=0}^{l} \tilde{\beta}_{p\,l}(1)\,\xi^p. \tag{A.6}$$

We denote

$$P_l(\xi) = \sum_{p=0}^{l} \tilde{\beta}_{p\,l}(1)\,\xi^p \tag{A.7}$$

and show that for BDFl, $l = 1, 2$, $P_l(\xi) = (-1)^l \prod_{p=1}^{l} (\xi - 1)$. From (A.4) we have

$$Re\,\{H(\mu)\}_{|\mu|=1} = \sum_{p=0}^{l} \beta_{p\,l}\,\cos\,(0 - p\,\phi). \tag{A.8}$$

Comparing the series $\sum_{p=0}^{l} \beta_{p\,l}\,\cos\,(0-p\,\phi)$ with (3.4), one can see that it corresponds to the discrete BDF l derivative operator for $f(t) = \cos\,(t)$:

$$Re\,\{H(\mu)\}_{|\mu|=1} = D_l \left[\frac{d\,\cos(t)}{d\,t}\right]_{t=0} \cdot \Delta\,t. \tag{A.9}$$

By construction of the discrete lth-order derivative operator with $\Delta t = \phi$,

$$Re\,\{H(\mu)\}_{|\mu|=1} = \frac{d\,\cos(t)}{d\,t}|_{t=0} \cdot \phi + O(\Delta t^{\,l}) \cdot \phi = O(\phi^{\,l+1}), \tag{A.10}$$

where $O(\phi^{\,l+1})$ are the terms of the order $l + 1$ and greater.

Now recall that $Re\,\{H(\mu)\}_{|\mu|=1}$ can be considered as an lth-order polynomial of $\xi = \cos\,(\phi)$, $P_l(\xi)$ (equations (A.6), (A.7)). According to the fundamental theorem of algebra, this polynomial has l roots and can be factorized as

$$P_l(\xi) = \tilde{\beta}_{ll}(1) \prod_{p=1}^{l} (\xi - \xi_p), \tag{A.11}$$

where ξ_p is the pth root of the polynomial. Expanding $\xi = \cos(\phi)$ in a Taylor series in ϕ, $\xi = 1 - \phi^2/2 + O(\phi^4)$, and substituting into (A.11), one gets

$$P_l(\xi) = \tilde{\beta}_{ll}(1) \prod_{p=1}^{l} \left(1 - \xi_p - \frac{\phi^2}{2} + O(\phi^4)\right). \tag{A.12}$$

Since $P_l(\xi) = Re\,\{H(\mu)\}_{|\mu|=1}$ contains only terms of $(l + 1)$th-order and higher in ϕ (cf. (A.10)), at least $\lceil (l + 1)/2 \rceil$ of its roots must be equal to one. For $l = 1, 2$, $\lceil (l+1)/2 \rceil = l$, meaning that *all* its roots are equal to one, and $P_l(\xi)$ can be factorized as

$$P_l(\xi) = (-1)^l \prod_{p=1}^{l} (\xi - 1), \tag{A.13}$$

since $\tilde{\beta}_{11}(1) = \beta_{11} = -1$ and $\tilde{\beta}_{22}(1) = 2\,\beta_{22} = 1$.

Now we show that the function $Re\{H(\mu)\} \geq 0 \; \forall |\mu| \leq 1$ for BDFl, $l = 1, 2$. We can write (A.5) as

$$Re\{H(\mu)\} = \sum_{p=0}^{l} \tilde{\beta}_{p\,l}(1)(r\,\xi)^p + \sum_{p=0}^{l} \beta'_{p\,l}(r)\xi^p, \tag{A.14}$$

where $\beta'_{p\,l}(r) = \tilde{\beta}_{p\,l}(r) - \tilde{\beta}_{p\,l}(1)\,r^p$. The first summand of (A.14), $\sum_{p=0}^{l} \tilde{\beta}_{p\,l}(1)$ $(r\,\xi)^p$, corresponds to the polynomial $P_l(r\,\xi)$ of (A.7). Using the factorization of (A.13), one can write $P_l(r\,\xi)$ for $l = 1$, 2 as

$$P_l(r\,\xi) = (-1)^l \prod_{p=1}^{l} (r\,\xi - 1) \geq 0, \tag{A.15}$$

since $r\,\xi = r\cos(\phi) \leq 1$ for $r \leq 1$. One can easily see that for $l = 1$, $\sum_{p=0}^{l} \beta'_{p\,l}(r)\xi^p = 0$, and for $l = 2$, $\sum_{p=0}^{l} \beta'_{p\,l}(r)\xi^p = \beta_{2\,2}(1 - r^2) \geq 0$ for $r \leq 1$, thus proving that $Re\{H(\mu)\} \geq 0 \; \forall |\mu| \leq 1$ for BDFl, $l = 1, 2$. Therefore, condition (A.2) implies $|\mu| > 1$, and the set U_1 contains only the eigenvalues $|\lambda| < 1$ for $s > 0$.

Set U_2. Now let us consider the set U_2 described by the condition (4.13). This condition means that $\lambda^\star$ lies inside the disk with the center at $\beta_{0\,l} + 2s$ and the radius of $s + s|G(\mu)|$. If $|G(\mu)| \leq 1$, the set $U_2 \subseteq U_1$ and thus contains only the eigenvalues with $|\lambda| < 1$ for $s > 0$by the previous analysis.

Now consider the case

$$|G(\mu)| > 1. \tag{A.16}$$

For the first-order interface extrapolation scheme, $m = 1$, $G(\mu) = \mu$ (equation 4.8), and (A.16) reads $|\mu| > 1$, that is, $|\lambda| < 1$.

Thus, both sets U_1 and U_2 contain only the eigenvalues with $|\lambda| < 1$ for BDFl, $l = 1, 2$, and $EXTm$, $m = 1$, which finishes the proof of the stability theorem.

The fact that the polynomial $P_l(\xi)$ of (A.7) can be factorized in the form (A.13) only for $l = 1, 2$ makes the proof unextendable to higher l cases. Indeed, for BDFl/EXTm schemes with $l > 2$ it is no longer true that $Re\{H(\mu)\} \geq 0 \;\; \forall \;\; |\mu| \leq 1$, that is, $\exists\, |\mu| \leq 1 : Re\{H(\mu)\} < 0$. For example, for $\mu = 0.97\,e^{\,i}$, $Re\{H(\mu)\} = -0.025$ for BDF3, $Re\{H(\mu)\} = -0.128$ for BDF4, and so on. Hence, the set U_1 might contain solutions with $|\mu| \leq 1$, or $|\lambda| \geq 1$.

For BDFl/EXTm schemes with $m > 1$ it is no longer true that $G(\mu) = \mu$. Therefore condition $|G(\mu)| > 1$ no longer implies $|\mu| > 1$. Thus, for the EXT2 scheme with $G(\mu) = 2\mu - \mu^2$, $\mu = i/2$ results in $|G(\mu)| = \sqrt{17}/4 > 1$. Hence, the set U_2 might contain solutions with $|\mu| \leq 1$, or $|\lambda| \geq 1$. These remarks imply that the proof of unconditional stability cannot be extended to the schemes with $l > 2$ and $m > 1$.

Appendix B. Derivation of a semidiscrete stability bound. In this appendix, we derive a semidiscrete stability bound given by (7.1). In the derivation, please keep in mind that quadratic stability bound $s < s_0^\star\, K^2$ in a discrete case corresponds to $\Delta\, t < s_0^\star\, \delta^2/\alpha$ in a semidiscrete case and a "small overlap size" condition $K/N < 1/2$ corresponds to $\delta/(a + \delta/2) < 1/2$.

For the BDFl schemes, the semidiscrete error propagation equation is the ordinary differential equation

$$\frac{d^2 z^n}{d\,x^2} = \frac{\beta_{0\,l}}{\alpha\,\Delta\,t}\, z^n, \tag{B.1}$$

where $z^n(x)$ is the error at time level t^n. Consider the left subdomain $[-a, \delta/2]$ (see Figure 3.1 for the domain sketch), since by symmetry the right subdomain possesses

the same solution with $x-a$ replaced by $a-x$. Equation (B.1) admits a general solution of the form $z_L^n(x) = A_1\, e^{-\sqrt{\frac{\beta_{0\,l}}{\alpha\Delta t}}\,x} + A_2\, e^{\sqrt{\frac{\beta_{0\,l}}{\alpha\Delta t}}\,x}$, where the subscript L stands for the left domain. Since $z_L^n(-a) = 0$, we get

$$z_L^n(x) = z_L^n(\delta/2)\,\frac{e^{\sqrt{\frac{\beta_{0\,l}}{\alpha\Delta t}}\,(x+a)} - e^{-\sqrt{\frac{\beta_{0\,l}}{\alpha\Delta t}}\,(x+a)}}{e^{\sqrt{\frac{\beta_{0\,l}}{\alpha\Delta t}}\,(\delta/2+a)} - e^{-\sqrt{\frac{\beta_{0\,l}}{\alpha\Delta t}}\,(\delta/2+a)}}. \tag{B.2}$$

Consider the overlap region $[-\delta/2, \delta/2]$, where the error dominates. For small overlap sizes $x + a \geq a - \delta/2 > 2\,a/3$ in the overlap region, and one can neglect the decaying exponent $e^{-\sqrt{\frac{\beta_{0\,l}}{\alpha\Delta t}}\,(x+a)}$ with respect to the growing exponent and write the solution as

$$z_L^n(x) \sim z_L^n(\delta/2)\, e^{\sqrt{\frac{\beta_{0\,l}}{\alpha\Delta t}}\,(x-\delta/2)}. \tag{B.3}$$

Let us follow the error propagation from $n = 0$ onward. To construct the solution for the first time level, we use a simple time-lagging scheme (or EXT1). Thus, boundary conditions are $z_L^1(\delta/2) = z_R^0(\delta/2) = z_L^0(-\delta/2)$ (subscript R stands for the right domain, and $z_L^0(x)$ and $z_R^0(x)$ represent initial error functions possessing $x-a \to a-x$ symmetry), and the error for the first time level in $[-\delta/2, \delta/2]$ is $z_L^1(x) \sim z_L^0(-\delta/2)\, e^{\sqrt{\frac{\beta_{0\,l}}{\alpha\Delta t}}\,(x-\delta/2)}$. If one continues with the EXT1 scheme, one obtains $z_L^n(x) \sim z_L^0(-\delta/2)\, e^{-(n-1)\sqrt{\frac{\beta_{0\,l}}{\alpha\Delta t}}\,\delta} e^{\sqrt{\frac{\beta_{0\,l}}{\alpha\Delta t}}\,(x-\delta/2)}$. Thus the error ratio is $||z_L^n(x)||_\infty / ||z_L^0(x)||_\infty \leq |e^{-(n-1)\sqrt{\frac{\beta_{0\,l}}{\alpha\Delta t}}\,\delta}| < 1$, making the EXT1 scheme stable for at least small overlap regions, for which neglecting the decaying exponent is justified. Our findings confirm this conclusion: EXT1 is unconditionally stable for BDF 1–2, is stable for BDF 3–5 for the considered range of parameters, and instabilities of BDF6/EXT1 were revealed only for large, and not for small, overlap sizes.

If we consider the EXT2 scheme, the boundary conditions at time step $n = 2$ will be

$$z_L^2(\delta/2) = 2\, z_L^1(-\delta/2) - z_L^0(-\delta/2) = z_L^0(-\delta/2)\left(2\, e^{-\sqrt{\frac{\beta_{0\,l}}{\alpha\Delta t}}\,\delta} - 1\right), \tag{B.4}$$

and the solution in $[-\delta/2, \delta/2]$ is $z_L^2(x) \sim z_L^0(-\delta/2)(2\, e^{-\sqrt{\frac{\beta_{0\,l}}{\alpha\Delta t}}\,\delta} - 1)\, e^{\sqrt{\frac{\beta_{0\,l}}{\alpha\Delta t}}\,(x-\delta/2)}$. Denoting $\xi = e^{-\sqrt{\frac{\beta_{0\,l}}{\alpha\Delta t}}\,\delta}$, we have $||z_L^2(x)||_\infty / ||z_L^0(x)||_\infty < 2\,\xi$. Proceeding with the EXT2 scheme, one gets $z_L^3(x) = z_L^0(-\delta/2)\,(4\,\xi^2 - 3\,\xi)\, e^{\sqrt{\frac{\beta_{0\,l}}{\alpha\Delta t}}\,(x-\delta/2)}$, and $||z_L^3(x)||_\infty / ||z_L^0(x)||_\infty < (2\,\xi)^2$. Proceeding similarly, one can obtain

$$||z_L^n(x)||_\infty / ||z_L^0(x)||_\infty < (2\,\xi)^{n-1}. \tag{B.5}$$

Analogously, one can show that in general for an EXTm scheme

$$||z_L^n(x)||_\infty / ||z_L^0(x)||_\infty < (\gamma_{1\,m}\,\xi)^{n-1}. \tag{B.6}$$

For a stable scheme, one needs $\gamma_{1\,m}\,\xi < 1$, leading for $\gamma_{1\,m} \neq 1$ to

$$\Delta\, t < \frac{s_0^\star}{\alpha}\,\delta^2, \;\; s_0^\star = \frac{\beta_{0\,l}}{\ln^2(\gamma_{1\,m})}. \tag{B.7}$$

Note that for large overlap sizes the decaying exponent $e^{-\sqrt{\frac{\beta_{0\,l}}{\alpha\Delta t}}\,(x+a)}$ in the solution

for the error can no longer be neglected in $[-\delta/2, \delta/2]$, since $a - \delta/2$ can be small, invalidating the previous analysis. Hence, the derived quadratic scaling of bound on Δt and stability of EXT1 scheme in a semidiscrete case applies only to small overlap sizes.

Acknowledgments. We thank Aleks Obabko for his useful suggestion and James Lottes for developing spectral interpolation routines which originated the current work.

REFERENCES

[1] M. J. Berger, *Stability of interfaces with mesh refinement*, Math. Comp., 45 (1985), pp. 301–318.
[2] C. Bernardi, Y. Maday, and A. T. Patera, *Domain decomposition by the mortar element method*, in Asymptotic and Numerical Methods for PDEs with Critical Parameters, H. G. Kaper and M. Garbay, eds., NATO Adv. Study Inst. C 384, EDP Sciences, Les Ulis, France, 1993, pp. 269–286.
[3] T. M. Burton and J. K. Eaton, *Analysis of a fractional-step method on overset grids*, J. Comp. Phys., 177 (2002), pp. 336–364.
[4] X.-C. Cai, *Multiplicative Schwarz methods for parabolic problems*, SIAM J. Sci. Comput., 15 (1994), pp. 587–603.
[5] M. H. Carpenter, J. Nordström, and D. Gottlieb, *A stable and conservative interface treatment of arbitrary spatial accuracy*, Math. Comp., 148 (1999), pp. 341–365.
[6] T. Chan and T. Matthew, *Domain decomposition algorithms*, Acta Numer., (1994) pp. 1–83.
[7] G. Chesshire and W. D. Henshaw, *Composite overlapping meshes for the solution of partial differential equations*, J. Comput. Phys., 90 (1990), pp. 1–64.
[8] C. N. Dawson, Q. Du, and T. F. Dupont, *A finite difference domain decomposition algorithm for numerical solution of the heat equation*, J. Comput. Phys., 90 (1990), pp. 1–64.
[9] M. Deville, P. Fischer, and E. Mund, *High-Order Methods for Incompressible Fluid Flow*, Cambridge University Press, Cambridge, UK, 2002.
[10] P. Fischer, *An overlapping Schwarz method for spectral element solution of the incompressible Navier-Stokes equations*, J. Comput. Phys., 90 (1997), pp. 84–101.
[11] C. Fletcher, *Computational Techniques for Fluid Dynamics*, Springer-Verlag, Berlin, 1991.
[12] J. Gao and G. He, *An unconditionally stable parallel difference scheme for parabolic equations*, Appl. Math. Comput., 135 (2003), pp. 391–398.
[13] B. Gustaffson, H.-O. Kreiss, and A. Sundstrøm, *Stability theory of difference approximations for initial boundary value problems:* II, Math. Comp., 26 (1972), pp. 649–686.
[14] B. Gustaffson, H.-O. Kreiss, and J. Oliger, *Time Dependent Problems and Difference Methods*, John Wiley & Sons, New York, 1995.
[15] M. Hinatsu and J. H. Ferziger, *Numerical computation of unsteady incompressible flow in complex geometry using a composite multigrid technique*, Intetnat. J. Numer. Methods Fluids, 13 (1991), pp. 971–997.
[16] J. Hozeaux and R. Codina, *A Chimera method based on a Dirichlet/Neumann coupling for the Navier-Stokes equations*, Comput. Methods Appl. Mech. Engrg., 192 (2003), pp. 3343–3377.
[17] S. Hahn, K. Duraisamy, G. Iaccarino, S. Nagarajan, J. Sitaraman, X. Wu, J. Alonso, J. D. Baeder, S. Lele, P. Moin, and F. Scmitz, *Coupled High-Fidelity URANS Simulation for Helicopter Applications*, Ann. Research Briefs, Center for Turbulence Research, Stanford, CA, 2006.
[18] K. Johannsen and D. Britz, *Matrix stability of the backward differentiation formula in electrochemical digital simulation*, Computers Chemistry, 23 (1999), pp. 33–41.
[19] S. G. Krantz, *Zero of Order n*, Handb. Complex Variables, Birkhäuser, Boston, 1999.
[20] D. Levy and E. Tadmor, *From semi discrete to fully discrete: Stability of Runge-Kutta schemes by the energy method*, SIAM Rev., 40, pp. 40–73.
[21] P. L. Lions, *On the Schwarz alternating method*, in Domain Decomposition Methods for Partial Differential Equations, R. Glowinski, G. H. Golub, G. A. Meurant, and J. Périaux, eds., SIAM, Philadelphia, 1988.
[22] M. Manna, A. Vacca, and M. O. Deville, *Preconditioned spectral multi–domain discretization of the incompressible Navier-Stokes equations*, J. Comput. Phys., 201 (2004), pp. 204–223.

[23] A. Mitchell, *Computational Methods in Partial Differential Equations*, John Wiley & Sons, New York, 1969.
[24] R. L. Meakin, *Composite overset structured grids*, in Handbook of Grid Generation, J. F. Thompson, B. K. Soni, and N. P. Weatherhill, eds., CRC Press, Boca Raton, FL, 1999, pp. 1–20.
[25] P. Moore and J. E. Flaherty, *Adaptive local overlapping grid methods for parabolic systems in two space dimensions*, J. Comput. Phys., 98 (1992), pp. 54–63.
[26] A. Qaurteroni and A. Valli, *Domain Decomposition Methods for Partial Differential Equations*, Oxford University Press, Oxford, UK, 1999.
[27] C. Pärt-Evander and B. Sjögreen, *Conservative and non-conservative interpolation between overlapping grids for finite volume solutions of hyperbolic problems*, Comp. Fluids., 23 (1994), pp. 551–574.
[28] L. F. Pavarino and O. B. Widlund, *A polylogarithmic bound for an iterative substructuring method for spectral elements in three dimensions*, SIAM J. Numer. Anal., 33 (1996), pp. 1303–1335.
[29] Y. V. Peet and S. K. Lele, *Computational framework for coupling compressible and low Mach number codes*, AIAA J., 46 (2008), pp. 1990–2001.
[30] Y. Peet and P. Fischer, *Conjugate Heat Transfer LES Simulations in Application to Wire-wrapped Fuel Pins*, AIAA, Chicago, IL, 2010
[31] W. Rivera-Gallego, *Stability analysis of numerical boundary conditions in domain decomposition algorithms*, Appl. Math. Comput., 137 (2003), pp. 375–385.
[32] W. Rivera, J. Zhu, and D. Huddleston, *An efficient parallel alrgorithm with application to computational fluid dynamics*, Comput. Math. Appl., 45 (2003), pp. 1965–1988.
[33] H. Rui, *Multiplicative Schwarz methods for parabolic problems*, Appl. Math. Comput., 136 (2003), pp. 593–610.
[34] J. U. Schlüter, X. Wu, S. Kim, S. Shankaran, J. J. Alonso, and H. Pitsch, *A framework for coupling Reynolds-averaged with large-eddy simulations for gas turbine applications*, J. Fluids Engrg., 127 (2005), pp. 806–815.
[35] H. A. Schwarz, *Gesammelte Mathematische Abhandlungen*, vol. 2, Springer-Verlag, Berlin, 1890, pp. 133–143.
[36] B. Smith, P. Bjørstad, and W. Gropp, *Domain Decomposition: Parallel Multilevel Methods for Elliptic PDEs*, Cambridge University Press, Cambridge, UK, 1996.
[37] H. S. Tang, S. C. Jones, and F. Sotiropoulos, *An overset grid methods for 3D unsteady incompressible flows*, J. Comput. Phys., 191 (2003), pp. 567–600.
[38] J. L. Steger and J. A. Benek, *On the use of composite grid schemes in computational aerodynamics*, Comput. Methods Appl. Mech. Engrg., 64 (1987), pp. 301–320.
[39] J. C. Strikwerda and C. D. Scarbnick, *A domain decomposition method for incompressible viscous flow*, SIAM J. Sci. Comput., 14 (1993), pp. 49–67.
[40] R. Varga, *Matrix Iterative Analysis*, Springer-Verlag, Berlin, 2000.
[41] Z. J. Wang, *A fully conservative interface algorithm for overlapped grids*, J. Comput. Phys., 122 (1995), pp. 96–106.
[42] Z. J. Wang and V. Parthasarathy, *A fully automated Chimera methodology for multiple moving body problems*, Internat. J. Numer. Methods Fluids, 33 (2000), pp. 919–938.
[43] Y. Zang and R. L. Street, *A composite multigrid method for calculating unsteady incompressible flows in complex domains*, Internat. J. Numer. Methods Fluids, 20 (1995), pp. 341–361.